AN INVESTIGATION OF THE REUSABILITY ON NI-BASED SUPERALLOY POWDERS DISCARDED FROM ADDITIVE MANUFACTURING

Master's Thesis

Yağmur Can GÜNDOĞAN

Eskişehir 2025

AN INVESTIGATION OF THE REUSABILITY ON NI-BASED SUPERALLOY POWDERS DISCARDED FROM ADDITIVE MANUFACTURING

Yağmur Can GÜNDOĞAN

MASTER'S THESIS

Department of Materials Science and Engineering

Supervisor: Assist. Prof. Dr. Umut SAVACI

Eskişehir

Eskişehir Technical University

Institute of Graduate Programs

August 2025

FINAL APPROVAL FOR THESIS

This thesis titled AN INVESTIGATION OF THE REUSABILITY ON NI-BASED SUPERALLOY POWDERS DISCARDED FROM ADDITIVE MANUFACTURING has been prepared and submitted by Yağmur Can GÜNDOĞAN in partial fulfillment of the requirements in "Eskişehir Technical University Directive on Graduate Education and Examination" for the Degree of Master of Science in Materials Science and Engineering Department has been examined and approved on 21/08/2025.

Committee Members		**Title, Name and Surname**	**Signature**
Member	:	Assist. Prof. Dr. Umut SAVACI	
Member	:	Prof. Dr. Hakan GAŞAN	
Member	:	Assoc. Prof. Dr. Erhan AYAS	

Prof. Dr. Harun BÖCÜK

Director of the Institute of Graduate Programs

21/08/2025

SUPERVISOR APPROVAL

Master's student Yağmur Can GÜNDOĞAN, whom I supervise, has completed this thesis titled AN INVESTIGATION OF THE REUSABILITY ON NI-BASED SUPERALLOY POWDERS DISCARDED FROM ADDITIVE MANUFACTURING. According to my inspections, the work is scientifically and ethically appropriate for the student to the thesis defense exam.

Supervisor

Assist. Prof. Dr. Umut SAVACI

ABSTRACT

AN INVESTIGATION OF THE REUSABILITY ON NI-BASED SUPERALLOY POWDERS DISCARDED FROM ADDITIVE MANUFACTURING

Yağmur Can GÜNDOĞAN

Department of Materials Science and Engineering

Eskişehir Technical University, Institute of Graduate Programs, August 2025

Supervisor: Assist. Prof. Dr. Umut SAVACI

Powders used in additive manufacturing progressively degrade into scrap due to storage conditions and repeated reuse. Although such scrap powders can technically be recycled and reintroduced into additive manufacturing, this practice generally offers economic benefits primarily to powder manufacturers who use scrap powder a raw material. For end users, however, recycling is often not cost-effective. Consequently, it becomes essential to develop alternative processing routes that allow end users to repurpose these scrap powders, thereby extending their usability beyond additive manufacturing applications. This study investigates the feasibility of employing scrap Inconel 718 powder in powder metallurgy and examines how its physical, chemical, mechanical, and metallurgical properties compare to those of virgin Inconel 718 powder.

Keywords: Reusability, Powder metallurgy, Hot isostatic pressing, Ni-based superalloy, Encapsulation.

ÖZET

KATMANLI İMALATTA YENİDEN KULLANILARAK HURDAYA AYRILMIŞ NİKEL BAZLI SÜPER ALAŞIM TOZLARININ YENİDEN KULLANILABİLİRLİĞİNİN ARAŞTIRILMASI

Yağmur Can GÜNDOĞAN

Malzeme Bilimi ve Mühendisliği Anabilim Dalı

Eskişehir Teknik Üniversitesi, Lisansüstü Eğitim Enstitüsü, Ağustos 2025

Danışman: Dr. Öğr. Üy. Umut SAVACI

Katmanlı imalatta kullanılan tozlar, saklama koşulları ve tekrarlı kullanımları sebebiyle zamanla hurda haline gelmektedir. Bu hurda tozlar geri dönüştürülerek yeniden katmanlı imalat süreçlerine dahil edilebilmektedir ancak bu durum maaliyet açısından hurda tozu ham malzeme olarak kullanan toz üreticisi için avantajlara sahip olsa da son kullanıcı için dezavantajlıdır. Dolayısıyla, hurda haline gelerek katmanlı imalatta kullanımı sonlanan bu tozların yeniden değerlendirilebilmesi olanak tanıyacak alternatif yöntemlere ve uygulama alanlarına ihtiyaç vardır. Bu çalışma, hurda haline gelmiş Inconel 718 tozunun toz metalurji yöntemi ile yeniden kullanılabilirliğini araştırmakta ve hurda tozun sergilediği fiziksel, kimyasal, mekanik ve metalurjik özelliklerin yeni Inconel 718 tozun sergilediği özellikler ile farklılıklarını incelemektedir.

Anahtar Sözcükler: Yeniden kullanılabilirlik, Toz metalurjisi, Sıcak izostatik presleme, Nikel bazlı süper alaşım, Kapsülleme.

ACKNOWLEDGEMENTS

To my dear mom and dad…

From the very first day of my master's journey, I've been fortunate to have the support of incredible colleagues. I want to sincerely thank each and every one of them for being there, both mentally and physically, throughout this process.

To my wonderful managers and teammates at the R&D and Innovation Department, your guidance during the early stages, especially when I was trying to shape my thesis topic, was truly invaluable. I'm deeply grateful to have had you by my side.

I feel incredibly lucky to have had Assist. Prof. Dr. İsmail Özgür ÖZER's support in bringing the experimental part of my thesis to life, especially considering how busy he was. His effort and dedication ment so much to me.

I also want to extend heartfelt thanks to my collegues in the Laboratory and Testing and Data teams. The long hours you devoted to supporting the production and testing of my thesis samples made everything much more manageable, I couldn't have done in without you.

A special thank you to my thesis supervisor, Assist. Prof. Dr. Umut SAVACI. Working with you has been one of the highlights of this journey. Your support, especially during the tougher moments, and everything I've learned from you have made a lasting impact.

During this intense period, I was also lucky to have a truly valuable person in my life, who helped me stay grounded and motivated when things felt overwhelming. Dr. Kübra GÜRCAN BAYRAK. I'm so glad our paths crossed. You've made more of a difference than you probably realize, and I hope you'll always be part of my life.

And finally, to my dear mom and dad… Where do I even begin? You've always believed in me, encouraged me to chase what would bring me joy, and pushed me to grow into the person I am today. Thank you for raising me to stand strong on my own, to work hard, and to stay true to my values. I love you more than words can express.

Yağmur Can GÜNDOĞAN

21/08/2025

STATEMENT OF COMPLIANCE WITH ETHICAL PRINCIPLES AND RULES

I hereby truthfully declare that this thesis is an original work prepared by me; that I have behaved in accordance with the scientific ethical principles and rules throughout the stages of preparation, data collection, analysis and presentation of my work; that I have cited the sources of all the data and information that could be obtained within the scope of this study, and included these sources in the references section; and that this study has been scanned for plagiarism with “scientific plagiarism detection program” used by Eskişehir Technical University, and that “it does not have any plagiarism” whatsoever. I also declare that, if a case contrary to my declaration is detected in my work at any time, I hereby express my consent to all the ethical and legal consequences that are involved.

Yağmur Can GÜNDOĞAN

CONTENTS

Page

LIST OF TABLES

Page

LIST OF FIGURES

Page

GLOSSARY OF SYMBOLS AND ABBREVIATIONS

AM	:	Additive manufacturing
BCT	:	Body-centered tetragonal
FCC	:	Face-centered cubic
GA	:	Gas atomization
HB	:	Brinnel hardness
HCP	:	Hexagonal close-packed
HCF	:	High cycle fatigue
HIP	:	Hot isostatic pressing
HR	:	Hausner ratio
IPA	:	Isopropyl
LPBF	:	Laser powder bed fusion
LCF	:	Low cycle fatigue
PA	:	Plasma atomization
PIM	:	Powder injection molding
PM	:	Powder metallurgy
PPBs	:	Prior particle boundaries
PREP	:	Plasma rotating electrode process
PSD	:	Particle size distribution
δ	:	Delta
γ'	:	Gamma prime
γ''	:	Gamma double prime

1. INTRODUCTION

Additive manufacturing technologies represent innovative production methods that facilitate the rapid fabrication of components with complex geometries and minimal material waste. Among these, powder bed fusion systems stand out as some of the most widely employed techniques. In such systems, metal powders are spread layer by layer and selectively melted using an energy source to build the final component. This approach offers substantial advantages, particularly for nickel-based superalloys commonly utilized in the aerospace and energy sectors. Of these alloys, Inconel 718 is especially noteworthy due to its mechanical performance.

However, certain limitations are inherent to both the production and reusing of metal powders in additive manufacturing. With each reuse cycle, powders undergo specific physical and chemical changes that progressively degrade their properties. These physical and chemical alterations directly affect the suitability of the powders for additive manufacturing. Once critical thresholds are exceeded, the powders are classified as scrap. Consequently, manufacturers must either dispose of these powders or return them to powder producers for re-atomization that costly process that primarily benefits powder manufacturers. For end-user companies engaged in additive manufacturing, this introduces an additional cost burden that negatively impacts overall production economics.

In this study, the principal factors contributing to the classification of Inconel 718 powders previously used in additive manufacturing as scrap were investigated. In the initial phase, comprehensive characterization of the powders was carried out to identify the key physical parameters and chemical parameters responsible for their rejection. Subsequently, these scrap powders were encapsulated in a capsule system as part of an alternative powder metallurgy approach and consolidated by hot isostatic pressing. Unlike direct reuse in additive manufacturing, this strategy targeted the recovery of these powders through a different manufacturing route. The same process was also applied to virgin Inconel 718 powders, enabling a comparative evaluation of the mechanical properties of the resulting products. The findings of this study provide a new perspective on repurposing powders classified as scrap in additive manufacturing and indicate that integrating powder metallurgy with hot isostatic pressing may offer a promising and economical alternative for reutilizing such waste materials.

2. BACKGROUND AND LITERATURE

In the following subsections, the properties of the Inconel 718 alloy are discussed, together with the factors that lead to the classification of powder feedstock as scrap after repeated use in additive manufacturing. In addition, the consolidation of powders through encapsulation and hot isostatic pressing is described, drawing on the information available in the literature.

2.1. Inconel 718 Alloy

Nickel-based superalloys stand out as the most sophisticated and extensively employed group of superalloys designed for service in high-temperature environments. They are predominantly used in gas turbines powering both commercial and military aircraft, as well as in power generation units and marine propulsion systems. Beyond these, they serve essential functions in the oil and gas industry, spacecraft, submarines, nuclear reactors, and advanced military electric motors. The development and adoption of particular chemical compositions within this alloy family have been largely driven by the continuous pursuit of materials that can endure ever-increasing operating temperatures without compromising mechanical strength or corrosion resistance [1]. An overview of the chemical composition of different Inconel superalloys as shown in Table 2.1.

Inconel 718 is a polycrystalline nickel-based superalloy with a face-centered cubic (FCC) structure, whose mechanical properties are substantially improved through precipitation hardening by the gamma prime (γ') and gamma double prime (γ'') phases.

This alloy is particularly noted for its exceptional strength and impressive fatigue resistance, along with its capability to retain structural integrity during extended exposure to elevated temperatures. These characteristics make Inconel 718 an essential material in aerospace engineering and various high-temperature industrial applications [3-5].

Table 2.1. *An Overview of the Chemical Composition of Different Inconel Superalloys*

	Elements (Min. / Max. (wt%))										
Alloy	**Mn**	**Si**	**P**	**Cr**	**Co**	**Mo**	**Nb+Ta**	**Ti**	**Al**	**Nb**	**Ta**
Inconel 718	-/	-/	-/	17.0/	-/	2.80/	4.75/	0.65/	0.20 /		
ASTM F3055	0.35	0.35	0.015	21.0	1.00	3.30	5.50	1.15	0.80		
Inconel 625	-/	-/		20.0/		8.0/	3.15/	-/	-/		
ASTM B443	5.0	5.0		23.0		10.0	4.15	4.0	4.0		
Inconel 939	-/	-/		20.0/	18.0/			-/	-/	-/	-/
[2]	0.5	0.5		23.0	20.0			4.0	2.0	1.2	2.0
	Fe	**Cu**	**Ni**	**B**	**C**	**S**	**O**	**W**	**Zr**		
Inconel 718	Bal.	-/ 0.30	50.0/ 55.0	-/ 0.006	-/ 0.080	-/ 0.015	-/ 0.030				
Inconel 625	-/ 5.0		-/ 58.00		-/ 1.0						
Inconel 939	-/ 0.5		Bal.	-/ 0.5	-/ 0.15	-/ 0.002		-/ 3.0	-/ 0.15		

The mechanical performance of Inconel 718 is largely dictated by its microstructural attributes, underscoring the importance of thoroughly understanding the roles played by chemical composition, processing parameters, and heat treatment procedures. The alloy's principal strengthening mechanism stems from the precipitation of metastable γ″ and γ′ phases, which remain coherent with the FCC γ matrix. To promote the fine-scale distribution of these phases -typically around 16% γ″ and 4% γ′ - carefully tailored heat treatment cycles are employed. Nonetheless, during high-temperature processing, niobium tends to segregate and foster the formation of the Laves phase. This phase detrimentally affects strength, ductility, fatigue life, and creep rupture resistance by depleting essential alloying elements (such as Ni, Fe, Cr, Mo, and Ti) that are crucial for precipitation hardening, and by providing sites that facilitate crack initiation and propagation. The risk is particularly pronounced when the Laves phase develops an elongated morphology, markedly increasing the alloy's susceptibility to hot cracking. Furthermore, excessive aging or prolonged thermal exposure can cause γ′ to transform into incoherent delta (δ) precipitates, a phenomenon well documented to undermine the mechanical robustness of the alloy [6,7].

Below is a summary of the phases observed in Inconel 718 along with their effects on its mechanical performance and microstructural characteristics:

- The γ matrix forms the principal FCC phase in Inconel 718, comprising a nickel-rich solid solution with significant chromium and iron content. This phase is fundamental to the alloy's inherent ductility and its excellent resistance to corrosion [5].
- The γ′ precipitates in Inconel 718 are FCC-structured intermetallic compounds with an approximate composition of Ni_3(Al, Ti, Nb). They maintain a high degree of coherency with the γ matrix and exhibit minimal lattice misfit. The formation and characteristics of γ′ are largely dictated by the alloy's niobium content and its thermal processing history, with heat treatment parameters playing a pivotal role in determining their volume fraction, size, and distribution. While γ′ contributes to elevated temperature strength by effectively hindering dislocation motion, its strengthening effect is somewhat limited by its relatively low volume fraction. Nevertheless, the combined precipitation of γ′ and γ″ phases induces coherency strains, localized lattice distortions at coherent interfaces, that significantly enhance the alloy's strength, hardness, and resistance to creep rupture [5,7,8].
- The γ″ precipitates in Inconel 718 are body-centered tetragonal (BCT) intermetallic compounds with an approximate stoichiometry of Ni_3(Nb, Ti). Although they remain coherent with the γ matrix, they exhibit a pronounced lattice misfit. The formation of γ″ is predominantly controlled by the alloy's niobium content and its thermal exposure history. Within the microstructure, these precipitates typically appear as ellipsoidal disks. Heat treatment parameters play a crucial role in dictating the volume fraction, size, and distribution of γ″, thereby directly influencing the mechanical properties of the alloy [5,9,10]. A study reported in the literature measured the diameters of γ″ and γ′ precipitates and established their correlations with temperature and exposure duration by employing the Larson-Miller parameter [9]. Another study highlighted the significant influence of homogenization on the precipitation kinetics during aging treatment. It was particularly observed that both the size and number density of the precipitates varied depending on the duration of the aging [10]. These precipitates constitute the primary contributors to precipitation strengthening, maintaining their effectiveness even at elevated temperatures due to their high volume fractions and the considerable coherency strains they introduce. This strengthening effect is especially pronounced in areas with increased niobium content [5,7,11].

- The metal carbide (M_xC_y) precipitates, where M generally represents Ti or Nb, display characteristics that depend on their size and specific composition. Fine carbides, roughly 200 nm in diameter, strengthen the alloy through precipitation hardening mechanisms. Conversely, larger carbides, on the order of 2 μm, can diminish ductility yet enhance creep resistance by obstructing grain boundary sliding [5].
- Titanium nitride (TiN) precipitates form a brittle, detrimental phase that reduces the low-cycle fatigue life of Inconel 718 by creating localized stress concentrations [5].
- Delta (δ) phases are orthorhombic intermetallic compounds with an approximate composition of $Ni_3(Nb,Ti)$. While thermodynamically stable, they are inherently brittle and display a pronounced lattice misfit with the γ matrix. Interestingly, δ phases and γ″ precipitates share the same chemical composition; however, extended exposure to high temperatures can promote the transformation of γ″ into δ phases. Morphologically, δ phases commonly appear as needle-like or plate-like structures [5,7].
- Laves phases are hexagonal close-packed (HCP), metastable intermetallic compounds generally represented by the formula $(Ni, Fe, Cr)_2(Nb, Mo, Ti)$. Characteristically brittle and relatively coarse, they are classified as topologically close-packed eutectic phases. Laves phases tend to form in microstructural regions with significant niobium segregation, which act as preferential sites for void and crack initiation, ultimately undermining the alloy's mechanical performance [5]. The presence of the Laves phase significantly reduces the ultimate tensile strength at room temperature and also impairs impact toughness, fracture toughness, and high-temperature ductility. Additionally, these phases can act as preferential sites for crack initiation and propagation, which in turn diminishes low-cycle fatigue (LCF) life and accelerates fatigue crack growth rates [12].

Inconel 718 is commonly produced via conventional casting followed by isothermal forging. However, its pronounced work-hardening tendency makes it particularly challenging to machine using traditional methods such as turning, milling, or broaching. Additionally, isothermal forging can lead to non-uniform deformation, potentially resulting in undesirable microstructures that significantly undermine the mechanical properties of the final wrought components [4]. Therefore, in order to minimize

deformations cause by conventional methods, more controlled production methods are essential.

The solution heat treatment specifications for wrought Inconel 718 are defined by SAE/AMS Standard 5662 [13]. Solution heat treatment followed by aging is carried out on the alloy in compliance with SAE/AMS Standard 5663. These thermal processes impart high tensile and fatigue strength, as well as excellent stress-rupture resistance [14]. Several studies in the literature indicate that Inconel 718 components fabricated through powder metallurgy (PM) or additive manufacturing (AM) are processed with the aim of satisfying the specifications set forth in SAE/AMS Standard 5663. Notably, NASA performed heat treatments on Inconel 718 parts produced via laser additive manufacturing in accordance with SAE/AMS 5663 and subsequently assessed their properties against the criteria established in both SAE/AMS Standards 5663 and 5664 [15]. Valencia et al. produced Inconel 718 components using powder injection molding (PIM), followed by hot isostatic pressing (HIP) and subsequent heat treatment in line with SAE/AMS Standard 5663. The yield and ultimate tensile strengths of all fabricated samples were then evaluated against the requirements specified in SAE/AMS Standard 5662 [16].

Superalloys manufactured by PM have been widely employed in the hot sections of turbine engines since the 1970s, owing to their outstanding mechanical properties and excellent resistance to high temperatures. In recent years, as-HIPed Inconel 718 has attracted significant interest because of its finer, more homogeneous microstructure and superior mechanical performance relative to its wrought counterpart. Moreover, as-HIPed alloys can be readily machined into near-net or net shapes, offering a cost-effective alternative to conventionally hot-worked alloys. Nonetheless, the formation of MC-type carbides along prior particle boundaries (PPBs) continues to pose a notable challenge in PM superalloys, as these precipitates can degrade mechanical properties. PPBs, typically formed during the HIP process, are characterized by thin layers of secondary phases that envelop the original powder particles. The presence of such boundaries is well documented to compromise critical mechanical attributes, including tensile strength and impact toughness [17]. Through the optimization of HIP parameters, the formation of carbides along PPBs in Inconel 718 can be effectively minimized, thereby alleviating this issue and improving the alloy's overall mechanical performance [3,18].

In addition to HIP, laser additive manufacturing techniques enable the direct manufacturing of three-dimensional metallic components with complex geometries and

desirable mechanical properties. Inconel 718 is especially well-suited for laser-based additive processes, owing to its inherently good weldability that is a characteristic largely attributed to its relatively low aluminum and titanium content [4,6]. The acceptance criteria for Inconel 718 powders and components fabricated through laser additive manufacturing are specified in ASTM Standard F3055 [19,20].

Xu et al. [21] explored the effects of HIP and subsequent heat treatment on the microstructure, phase composition, and mechanical properties of Inconel 718 produced by laser additive manufacturing. In their study, HIP was carried out at 1150 °C for 4 hours under 1500 bar of argon pressure, followed by heat treatment in accordance with SAE/AMS Standard 5662. The results demonstrated that HIP effectively eliminated Laves phases and promoted the formation of ultra-fine nanoscale γ″ precipitates. Subsequent heat treatment facilitated the growth of these γ″ precipitates, leading to a coarser distribution within the microstructure. The combined removal of deleterious Laves phases and enhanced precipitation of γ″ was shown to positively impact the alloy's mechanical performance. Notably, the yield strength improved significantly, from 738 MPa in the as-built condition, to 1015 MPa after heat treatment, and reaching 1184 MPa following the combined HIP and HT process.

Rao et al. [22] consolidated Inconel 718 powder using HIP conducted at 1200 °C under 120 MPa for 3 hours, and subsequently examined the resulting microstructure and mechanical properties. Archimedes density measurements revealed an approximate relative density of 100%. Optical microscopy identified PPBs within the matrix, which, due to the elevated oxygen content of the starting powder, primarily comprised Al_2O_3 and TiO_2 phases. Additionally, MC-type carbides enriched with Nb and Ti were detected along these PPBs. Mechanical testing at room temperature showed a yield strength of 993 MPa, an ultimate tensile strength of 1337 MPa, and an elongation of 19.4%, values that are comparable to those specified for wrought Inconel 718 under SAE/AMS Standard 5662.

2.2. Powder Reuse and the Mechanisms Behind Scrap Generation in Additive Manufacturing

AM is a production method that builds three-dimensional components by progressively adding material, fundamentally differing from traditional subtractive

techniques. Of the various AM processes, laser powder bed fusion (LPBF) has become the most widely adopted worldwide. In LPBF, a thin layer of metal powder is spread to create a powder bed with a controlled packing density, which is then selectively melted by a high-power laser to form the intended geometry. The remaining unmelted powder not only supports the developing structure but also undergoes repeated thermal cycles, particularly in regions near the melt pool, throughout the layer-by-layer fabrication process [23].

Since only a portion of the powder bed is ultimately fused into the final component, the remaining unmelted powder acts as a support medium and can be recycled across multiple build cycles until it no longer conforms to the specifications required for AM feedstock. The reusability of such powders is governed by various factors, including thermal exposure, oxidation, and repeated handling. Over successive reuse cycles, these powders may experience degradation in their chemical composition, purity, or physical properties, eventually reaching a point where they fail to meet AM powder standards and must be designated as scrap [24].

There are currently several metal powder atomization methods that enable powder production for AM, which include water atomization, gas atomization, centrifugal atomization, and plasma atomization. In metallurgical terminology, atomization refers to the process by which a molten metal stream is disintegrated into fine droplets, subsequently solidifying into powder particles [24].

Atomization typically consists of two primary stages. In the first stage, molten metal is disrupted and broken down into smaller droplets by high-velocity gas or water streams, plasma jets, or centrifugal forces. During the subsequent stage, these droplets rapidly cool. Initially, a large volume of molten metal is transformed into fine droplets through the shear forces imparted by the chosen atomization medium. As the process progresses, the droplets gradually adopt a near-spherical morphology before solidifying into the final metal powders. The efficiency and kinetics of atomization are heavily influenced by the temperature of the superheated droplets and the surface tension of the molten metal [25].

Gas atomization (GA) is a well-established technique for producing near-spherical metal powders. In this process, the raw material, either as elemental or pre-alloyed ingots or rods, is melted in a ceramic or water-cooled copper crucible using electric arc or induction heating. The molten metal is held briefly to achieve chemical homogeneity

before being allowed to flow freely or directed through a narrow refractory nozzle into an atomization chamber under high pressure. Inside the chamber, a high-velocity jet of inert gas, typically argon or nitrogen (though air or helium may also be used), breaks the melt into fine droplets. Water atomization operates on similar principles but employs a high-pressure water stream as the atomizing medium. This leads to intense heat transfer and momentum exchange, producing splashed droplets. Compared to GA, water atomization utilizes jets with much higher mass flow rates and heat capacities, resulting in powders that often exhibit greater irregularity and porosity. Nonetheless, this method is widely favored due to its lower cost and high throughput, achieving production rates up to roughly 1 ton per minute. It remains the dominant process for manufacturing ferrous metal powders as well as reactive materials like nickel-based alloys, copper, and copper alloys. Plasma atomization (PA) was developed to produce highly spherical powders of reactive metals, typically with average particle sizes around 40 μm. This technique combines melting and atomization into a single step, using an argon plasma jet that can reach temperatures up to 11,000 K. Such extreme temperatures prevent premature solidification, thereby minimizing the formation of irregular particle shapes. In the plasma rotating electrode process (PREP), a variant of centrifugal atomization, the feedstock is supplied as a rotating electrode rod, spinning at around 15,000 rpm, while being melted by a plasma arc. The centrifugal forces generated propel the molten droplets outward, allowing them to solidify into spherical powders before reaching the chamber walls [24].

Powder characteristics such as particle size distribution (PSD), flowability, and sphericity are critical in governing the spreadability and recoatability of powders during the LPBF process, which in turn directly affect the density, microstructure, and mechanical performance of the fabricated components. PSD quantifies the distribution of particle sizes within a powder batch and has a direct influence on the packing density achievable during layer deposition. For LPBF applications, powders generally exhibit a PSD in the range of 20 to 45 μm. The most widely used method to evaluate PSD is laser diffraction analysis performed with a laser particle size analyzer. Sphericity describes how closely powder particles resemble an ideal sphere. Spherical particles are highly desirable, as they have the lowest surface area-to-volume ratio compared to irregular geometries, which reduces surface friction and enhances flow behavior. Flowability pertains to the ease with which powders can flow, a property essential for achieving

consistent powder spreading in LPBF. Sufficient flowability ensures uniform layer deposition, resulting in consistent layer thickness, improved packing density, and more homogeneous absorption of laser energy. Collectively, these factors contribute to higher part density and superior mechanical properties in the finished build [26].

The flowability of metal powders is commonly characterized by the Hausner ratio (HR), which is calculated as the ratio of tapped density to apparent density. To determine HR, both densities must first be measured: apparent density is typically assessed following ASTM B212, whereas tapped density is measured in accordance with ASTM B527. The resulting HR value as shown in Figure 2.1 serves as an indicator of powder flow behavior, with lower ratios generally reflecting superior flowability [27-29].

Flow character	Hausner ratio
Excellent	1.00 – 1.11
Good	1.12 – 1.18
Fair	1.19 – 1.25
Passable	1.26 – 1.34
Poor	1.35 – 1.45
Very poor	1.46 – 1.59
Very, very poor	> 1.60

Figure 2.1. *Correlation between the HR and the flow character [45]*

The Hall flowmeter is widely utilized in the powder metallurgy industry as a standard method for characterizing powders. It measures the time required for a specified mass of powder to flow under gravity through the orifice of a standardized funnel, which is open to atmospheric pressure at both ends. This technique enables the determination of the average mass flow rate, as well as the apparent density of the powder. Flow measurements are typically performed in accordance with ASTM B213 [30,31].

Chemical composition refers to the precise concentrations of individual elements present within the powder. For many AM applications, it is crucial that the powder's composition strictly adheres to the alloy specifications required for the target material. In cases involving powder reuse or processing conditions that might alter the elemental balance, verifying the chemical composition becomes especially critical. Even slight

deviations can significantly impact the density, phase distribution, and mechanical properties of the final manufactured parts [26].

For Inconel 718 alloy powders to be deemed suitable for AM, they must comply with the requirements set forth in ASTM F3055; otherwise, they are classified as scrap. According to this standard, the chemical composition of the powders must lie within the specified ranges as shown in *Table **2.1***, and the powders must also demonstrate free-flowing behavior. These critical attributes can be affected not only by the initial powder production method but also by subsequent storage conditions.

Degradation processes such as contamination, thermal exposure, or partial sintering may significantly alter the properties of metal powders, leading to non-conformance with ASTM F3055 and thus necessitating their categorization as scrap. Typically, powders that fail to meet the standard are excluded from direct reuse in AM. The most common approach to recycle such material involves blending the scrap powder with virgin powder to recover acceptable properties before returning it to production. However, this method is generally unsuitable for high-specification applications, such as those in the aerospace industry. Alternatively, scrap powders can be re-atomized and fed back into the primary powder manufacturing process [32,33]. However, this approach is typically impractical for end users of the powder. Consequently, the possibility of repurposing such scrap powders, which are unsuitable for additive manufacturing, should be investigated through alternative manufacturing routes.

2.3. Powder Encapsulation and Consolidation Using Hot Isostatic Pressing

PM is a well-established manufacturing technique that utilizes metal powders, or blends of metal and non-metal powders, as raw materials to produce bulk metallic materials, composites, and a wide range of product forms. This is accomplished through a sequence of processes encompassing powder production, compaction, sintering, and subsequent secondary or finishing operations [34-37].

PM is extensively utilized across a wide array of industries, spanning from automotive to advanced aerospace applications. PM components have gained prominence as a cost-effective alternative to parts manufactured by traditional manufacturing methods and, in many instances, offer the only practical means for producing components that cannot be manufactured by other techniques.

The engineering applications of PM can generally be classified into three principal categories. The first includes products that are virtually impossible to manufacture using conventional processes, such as porous bearings, filters, bimetallic immiscible copper-lead alloys for bearing applications, and hard or soft magnetic components. The second category comprises items made from materials that are difficult to process by other means, such as components derived from tungsten- and molybdenum-based alloys. The third encompasses parts like small gears and connecting rods, where powder metallurgy serves as a highly efficient and economical alternative to conventional casting and forging methods [36].

HIP is a key PM technique used to consolidate and densify metallic powders into solid components at temperatures below their melting point, employing heated inert gases such as argon or nitrogen under extremely high pressures. This process facilitates the production of fully dense, near-net-shape parts from metal, ceramic, or composite powders [38-40].

HIP offers numerous advantages, including the elimination of macro and micro size porosity in cast materials; the attainment of theoretical density in sintered powders while minimizing excessive grain growth; and the densification of encapsulated powders to near-theoretical values, effectively preventing segregation and limiting grain coarsening. Additionally, HIP enables the joining of similar or dissimilar materials through solid-state diffusion bonding and facilitates compound synthesis via exothermic reactions that occur during the heating cycle [40].

Compaction imparts the initial shape to a metal powder component; however, its mechanical properties in the green state require enhancement through sintering, which promotes interparticle bonding by providing thermal energy. When compacted metal powders undergo sintering, typically at temperatures exceeding roughly half their absolute melting point, they begin to coalesce, forming necks at the contact points between particles. The migration of atoms toward these neck regions reduces the system's overall surface area, thereby lowering its total surface energy. The sintering of metal powders is predominantly governed by diffusion processes that proceed along thermally activated surface, grain boundary, or lattice pathways. In particular, surface and volume diffusion contribute to the rounding of pores within the compact, while grain boundary and volume diffusion are chiefly responsible for densification and the accompanying shrinkage of the structure [41].

In HIP, a thin-walled capsule, commonly called a can, canister, container, or mould, is filled with metal powder, then evacuated and hermetically sealed before being subjected to elevated temperatures and high isostatic pressures for prolonged periods. This process results in a fully densified component that is produced either in net shape or near-net shape form [42].

The encapsulation stage is crucial for the successful production of components from metal powders using HIP [43]. In the HIP process, employing a suitable encapsulation technique is essential to ensure that the gas, acting as the pressure transmitting medium, remains entirely isolated from the metal powder. As a result, preparing metal powders for HIP involves several critical steps: designing and fabricating the capsule, filling and sealing it (typically through welding), carrying out the HIP cycle, and finally removing the capsule along with performing any necessary secondary operations [41].

To produce near-net-shape components from metal powders via HIP, secondary processes such as mechanical machining or chemical treatments are often required to compensate for dimensional deviations introduced by the encapsulation process [41-44].

The materials selected for capsule production must exhibit both high strength and adequate ductility to accommodate plastic deformation, thereby enabling them to withstand the elevated pressures encountered during HIP. Stainless steels and mild steels are commonly chosen for this role due to their favorable balance of strength and ductility. Throughout the HIP process, the capsule is exposed to high temperatures and uniform isostatic stresses while also accommodating volumetric shrinkage, all while serving as an effective barrier that shields the metal powder from the external environment. The wall thickness of the capsule is a critical factor in the success of the HIP process. It must be sufficient to prevent cracking or structural failure under the demanding processing conditions, yet not so excessive as to hinder the required plastic deformation [41,43].

Metal encapsulation is a widely preferred method in the HIP process, although its use is generally limited to relatively simple geometries [41]. For small products and capsule designs with straightforward geometries, such as rectangular or cylindrical shapes, volumetric shrinkage during HIP can be estimated relatively easily. However, producing near-net-shape components with full theoretical density often requires the use of more complex capsule geometries. Since HIP is generally applied to manufacture only a limited number of large or geometrically intricate components, predictive models become crucial for estimating volumetric shrinkage in these cases. Such models assist in

designing suitable capsules for complex or oversized parts, ensuring dimensional precision and complete densification [43]. Advancing capsule designs to incorporate more complex geometries and larger dimensions will enhance the benefits of HIP, enabling the fabrication of near-net-shape components that achieve full theoretical density. Consequently, continued research in this area is essential.

According to the existing literature, numerous stringent criteria dictate the suitability of powder feedstocks for AM, particularly when targeting the production of high-quality, aviation-grade components. Consequently, substantial amounts of used powder often must be discarded and replaced with virgin feedstock, leading to significant economic implications. To mitigate these costs, repurposing scrap powders becomes essential. The HIP process, with its distinct advantages, offers a promising pathway to reincorporate such otherwise unusable scrap powders into manufacturing streams.

To evaluate the feasibility of employing scrap powders, previously utilized in AM, as feedstock for PM techniques like HIP, it is vital to investigate the properties of the resulting consolidated materials. The primary objectives of this study are to demonstrate the reusability of scrap powders through PM, to examine how processing parameters affect both virgin and scrap powders, and to explore potential application areas based on the mechanical and metallurgical properties of components produced from scrap feedstocks.

Accordingly, in this work, virgin and scrap Inconel 718 powders were encapsulated and subsequently consolidated by HIP under identical conditions. The consolidated materials were then subjected to detailed microstructural and mechanical characterization to assess the impact of powder type on the final properties.

3. EXPERIMENTAL STUDY

In this study, billets were fabricated via powder metallurgy using commercially available Inconel 718 powders. Both virgin Inconel 718 powders and powders rendered scrap due to reuse and prolonged storage under ambient conditions were employed as starting raw materials. These powders were loaded into capsules manufactured from stainless steel sheets through an encapsulation process, then consolidated into bulk samples by HIP. The resulting bulk samples underwent solution and aging heat treatments.

The experimental study began with a comprehensive characterization of the virgin and scrap Inconel 718 powders, which, through various characterization techniques, confirmed that the scrap powders did not meet the powder specifications specified in ASTM F3055.

The characterization methods applied to the virgin and scrap powders, as well as to the as-HIPed billets, and the corresponding referenced standards are summarized in

Table 3.1. Further details of the production process are provided in the following subsections.

Table 3.1. *The characterization methods applied to the virgin and scrap powders and as-HIPed billets*

	Material Form			
	Powder	**Standarts**	**Bulk**	**Standarts**
Characterization Methods	Scanning Electron Microscopy	NA	Archimedes Density	ASTM B311
	X-Ray Fluorescence	NA	Hardness Test	ASTM E10
	X-Ray Diffraction	NA	Optical Light Microscopy	NA
	O/N Elemental Analysis	ASTM E1019	Scanning Electron Microscopy	NA
	Appearent Density	ASTM B212	X-Ray Diffraction	NA
	Tap Density	ASTM B527	O/N Elemental Analysis	ASTM E1019
	Flow Rate	ASTM B213	Arc/Spark Optical Emission Spectrometry	ASTM E3047
	Particle Size Distribution	ASTM B822	Room Temperature Tensile Test	ASTM E8/E8M
			Elevated Temperature Tensile Test	ASTM E21
			High Cycle Fatigue Test	ASTM E466
			Stress-Rupture Test	ASTM E139

3.1. Materials and Method

The experimental study began with the characterization of virgin and scrap Inconel 718 powders to assess their properties. These analyses evaluated the morphology, surface texture, chemical composition, particle size distribution, apparent and tap densities, as well as the flow rates of the raw powders.

Capsules were manufactured by cutting 304 stainless steel (SS) sheets to the required dimensions and welding them together using 304 SS filler along with vent tubes. Leak tests were then performed to verify the integrity of the assembled capsules. Once leak tightness was confirmed, the capsules were filled with equal proportions of virgin and scrap Inconel 718 powders. The fill ports were sealed by cap welding to ensure airtightness, and the vent tubes were connected to a vacuum system.

Following evacuation, the vent tubes were sealed to maintain vacuum conditions, and the capsules were subjected to the HIP. The resulting as-HIPed billets were subsequently machined on a lathe to remove the outer 304 stainless steel layer. Blank samples were then extracted from the billets using electrical discharge machining (EDM). These blanks underwent solution and aging heat treatments, followed by precision turning to achieve their final geometries. The entire process flow for billet production employed in this study is depicted in Figure 3.1.

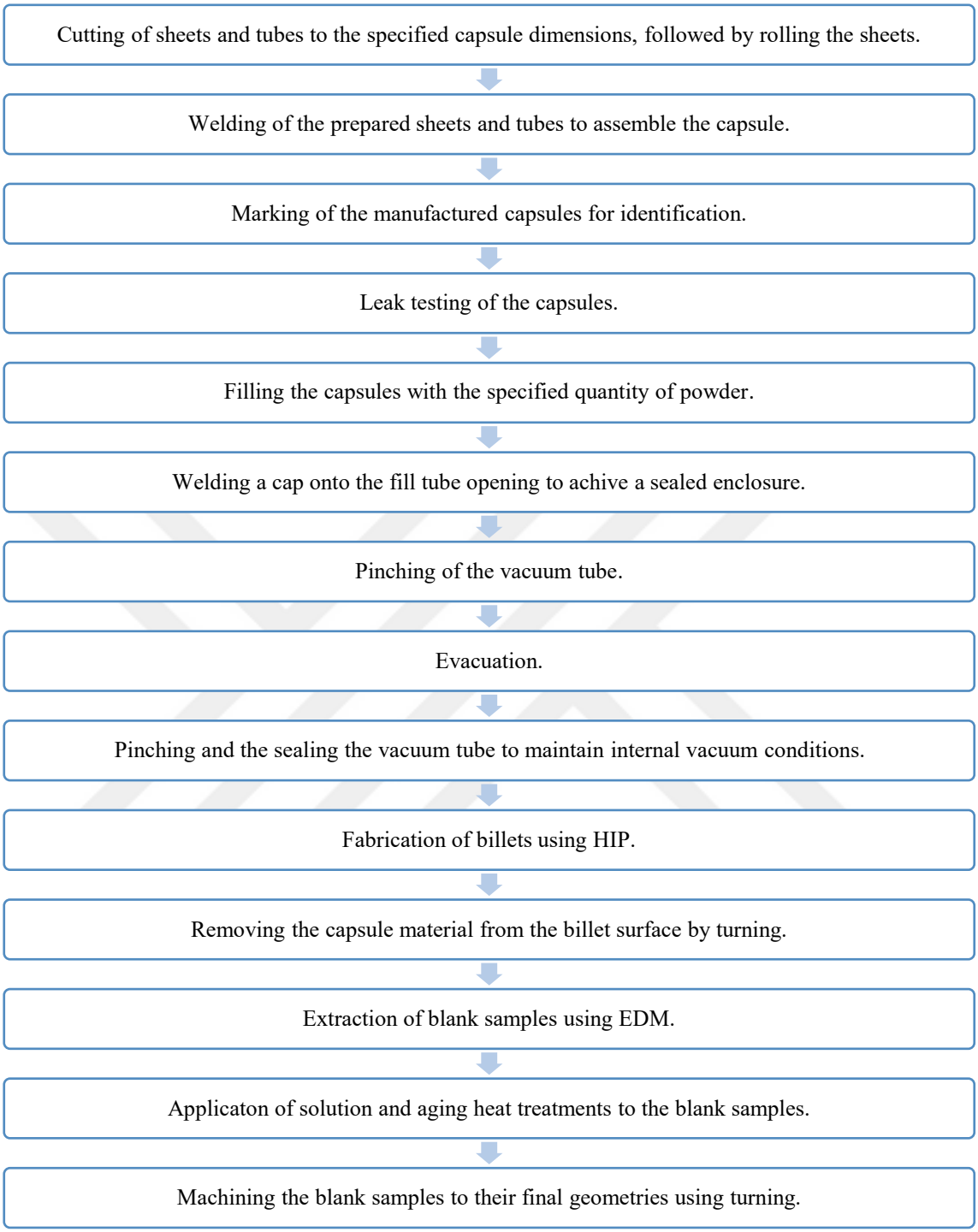

Figure 3.1. *Flow chart of billet production*

3.1.1. Preparation and fabrication of the capsules

Stainless steel sheets (304 SS) with a thickness of 1.525 mm were cut to the dimensions specified in Figure 3.2a using a laser cutting machine. The resulting sheets, shown in Figure 3.2b, were designated for capsule fabrication. These rectangular sheets

were then rolled with a metal slip roller to achieve the diameter indicated in the technical drawing presented in Figure 3.3.

Any burrs and contaminants introduced during cutting and rolling were removed by cleaning the surfaces with pressurized water followed by isopropyl alcohol (IPA). The rolled sheets were then assembled with the bottom and top caps, as well as the tubes, and welded together using Gas tungsten Arc Welding (TIG).

Subsequently, the capsules were labeled by laser marking: “718_V” for the capsule intended to be filled with virgin powder, and “718_S” for the one designated for scrap powder. Leak tests were then conducted by sealing the powder fill tube, pressurizing the capsule through the vent tube up to 2 bar with air, and immersing the assembly in water to detect any pressure drops or bubble formation, which would indicate leaks. The technical drawing detailing the fabricated capsule design is provided in Figure 3.3.

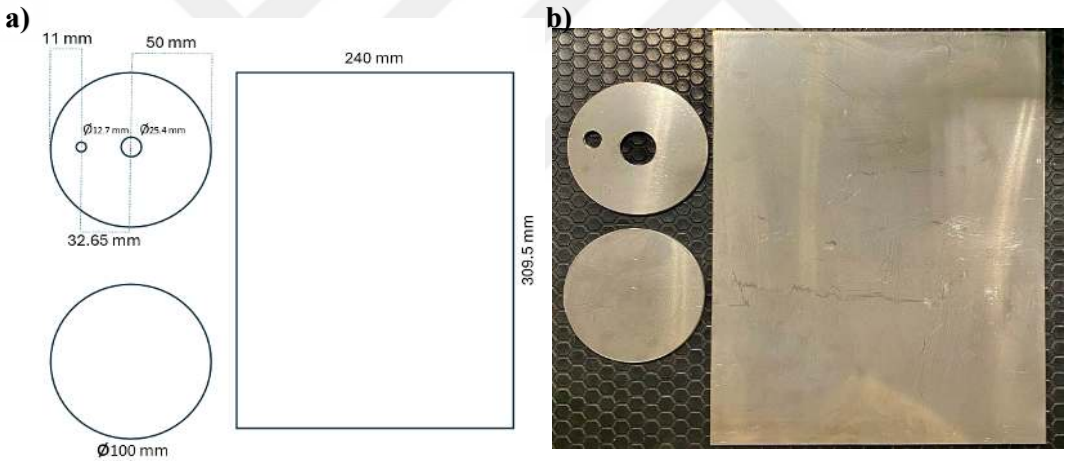

Figure 3.2. *a) Specified dimensions for the sheet layouts; b) sheets cut to these dimensions using laser cutting*

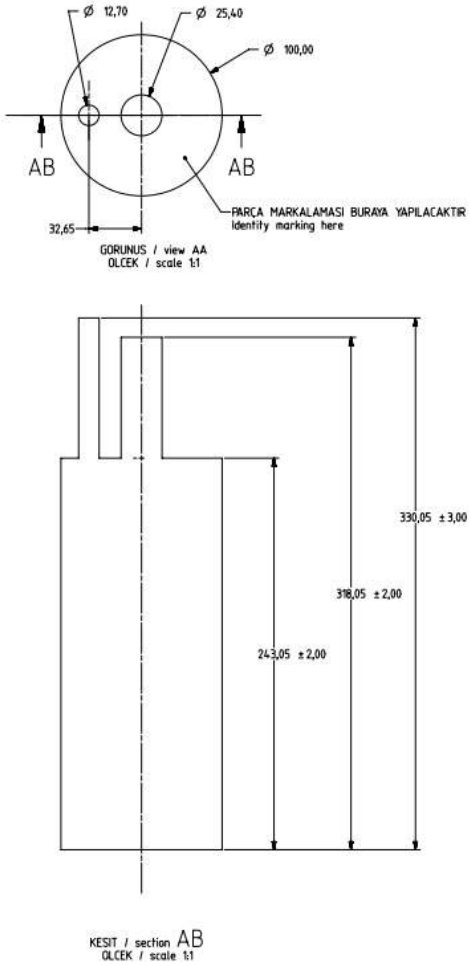

Figure 3.3. *Technical drawing illustrating the capsule design*

3.1.2. Filling of the capsules with powder

A total of 9,875.5 g of virgin and scrap Inconel 718 powders were introduced into the capsules through the fill tubes, resulting in a volumetric packing density of 67.98%. During the filling process, vibration motors capable of generating motion along both horizontal and vertical axes were utilized to dislodge trapped air and promote uniform powder settling within the capsules, thereby minimizing voids.

Upon completion of the filling, the fill tubes were sealed with 304 SS caps and hermetically closed using TIG welding. The final weight of the filled capsules was recorded as 11,080 g. An image of the fully filled capsules is provided in Figure 3.4.

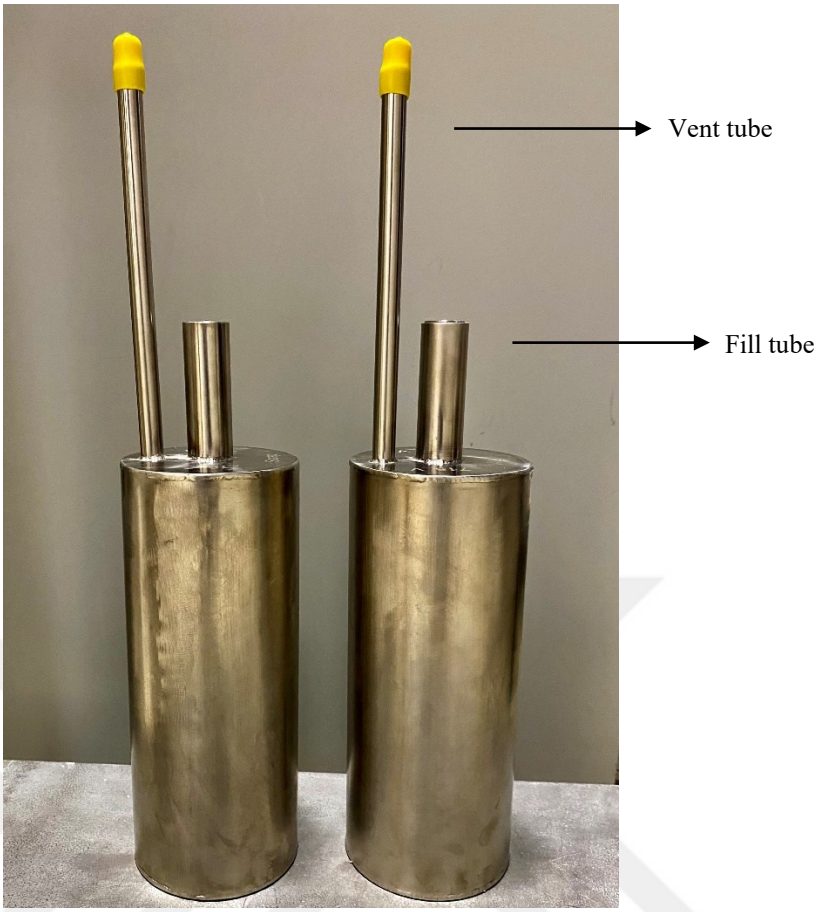

Figure 3.4. *Capsules Filled with Powder*

3.1.3. Evacuation

Prior to the HIP process, the vent tubes integrated into the capsules were connected to a vacuum system equipped with rotary vane pumps to evacuate trapped air, thereby promoting high densification during HIP. To prevent powder from being drawn out during evacuation, the vent tube was initially partially pinched using flat crimping jaws. Steel wool was then inserted above this first crimp to function as a filter, followed by a second crimp applied above the steel wool using flat jaws.

The evacuation was commenced and continued until the internal pressure stabilized at approximately 5×10^{-3} Torr. Once the target vacuum level was reached and maintained, the section of the vent tube above the steel wool was sealed by heating it with an oxy-acetylene torch, then crimped at three separate locations using toothed crimping jaws to ensure hermetic sealing. Figure 3.5 presents illustrations of the flat and toothed crimping jaws utilized during this procedure.

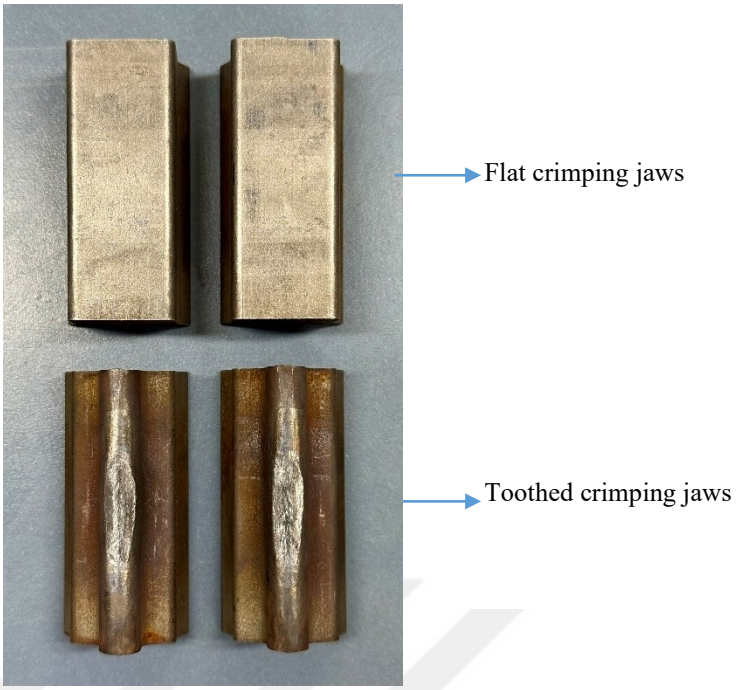

Figure 3.5. *Image of the flat and toothed crimping jaws used in the sealing process*

3.1.4. Hot isostatic pressing

The filled and hermetically sealed capsules were placed vertically in the HIP chamber with their tubes oriented upward, arranged side by side. HIP was carried out by heating the capsules at a rate of 10°C/min up to a maximum temperature of 1180°C, where they were maintained under a pressure of 150 MPa for 4 hours. Upon completion of sintering, the system was cooled to room temperature at the same rate of 10°C/min.

The chosen HIP parameters were determined based on relevant literature and prior experimental studies [1,2]. Dimensional measurements of the capsules taken before and after HIP are summarized in Table 3.2, while images of the capsules following HIP are shown in Figure 3.6.

Table 3.2. *Dimensions of the capsules measured before and after HIP*

Conditions	Height (mm)	Diameter (mm)
Before HIP	243.05	100.00
After HIP	216.00	87.20

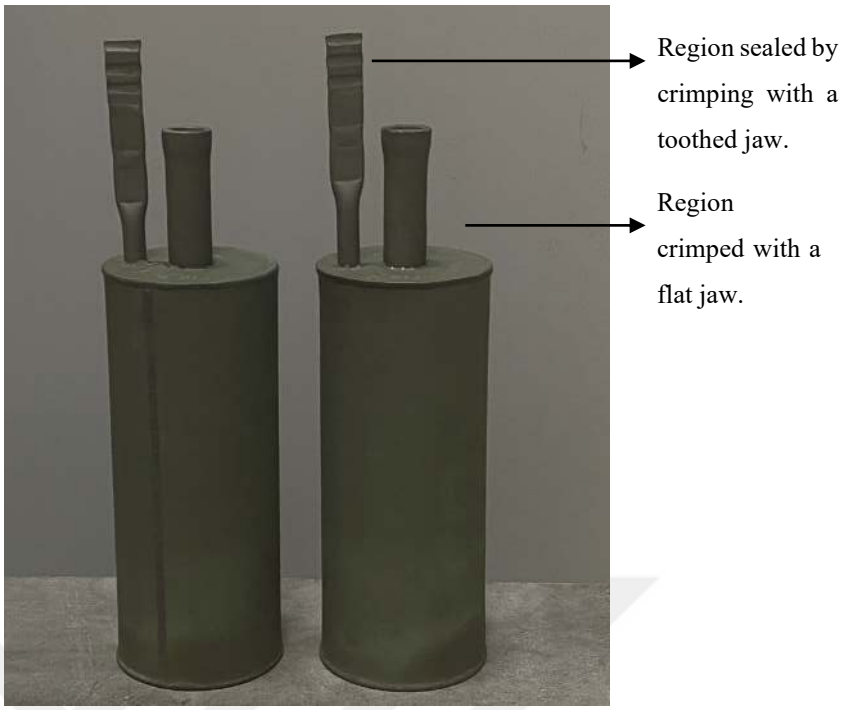

Figure 3.6. *Image of the capsules after HIP*

3.1.5. Surface machining by turning

To remove the 304 stainless steel layer that diffused into the billet surfaces during sintering, the as-HIPed capsules were subjected to turning operations. Prior to machining, the fill and vent tubes were cut off and removed from the capsules. The dimensions of the billets before and after turning are summarized in Table 3.3, while an image of the machined billets is provided in Figure 3.7.

Table 3.3. *Dimensions of billets before and after turning*

Conditions	Height (mm)	Diameter (mm)
Before Turning	216.00	87.20
After Turning	212.50	83.00

Figure 3.7. *Billets with surfaces machined by turning*

3.1.6. Extraction of blank samples from billets by EDM

To enable a comparative evaluation of the physical, mechanical, and metallurgical properties of billets produced from virgin and scrap Inconel 718 powders, blank samples were extracted using electrical discharge machining (EDM). The EDM process employed a 0.3 mm diameter copper wire with deionized water serving as the cooling medium.

The locations within the billets from which blank samples were removed for room temperature tensile (RT), elevated temperature tensile (ET), stress-rupture, and high cycle fatigue (HCF) tests are illustrated in Figure 3.8, Figure 3.10, and Figure 3.11. The sampling positions for Archimedes density, SEM, and microhardness analyses are shown in Figure 3.12. The sample codes corresponding to these different regions and analyses are provided in Table 3.4, Table 3.5, and Table 3.6.

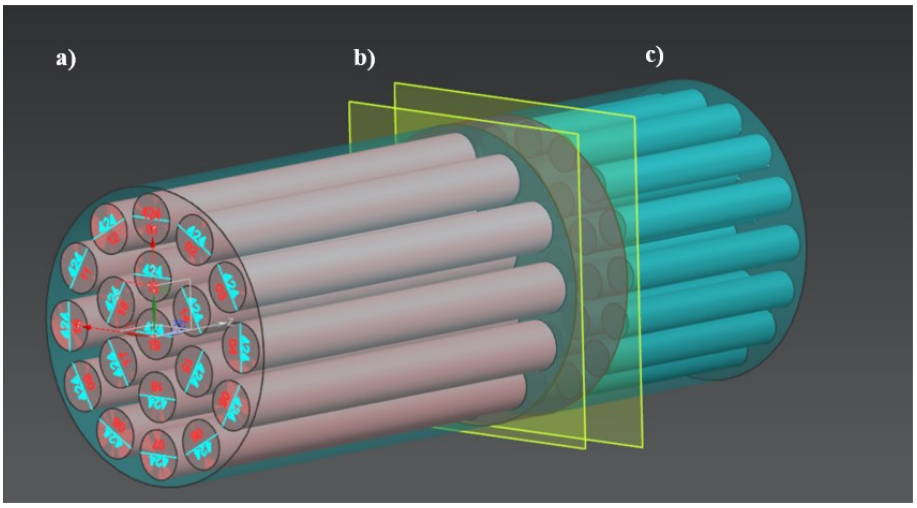

Figure 3.9. *Location of blank samples within the billet: (a) region containing samples for HCF testing; (b) region containing samples for Archimedes, SEM, and microhardness analyses; (c) region containing samples for RT tensile, ET tensile, and stress-rupture tests*

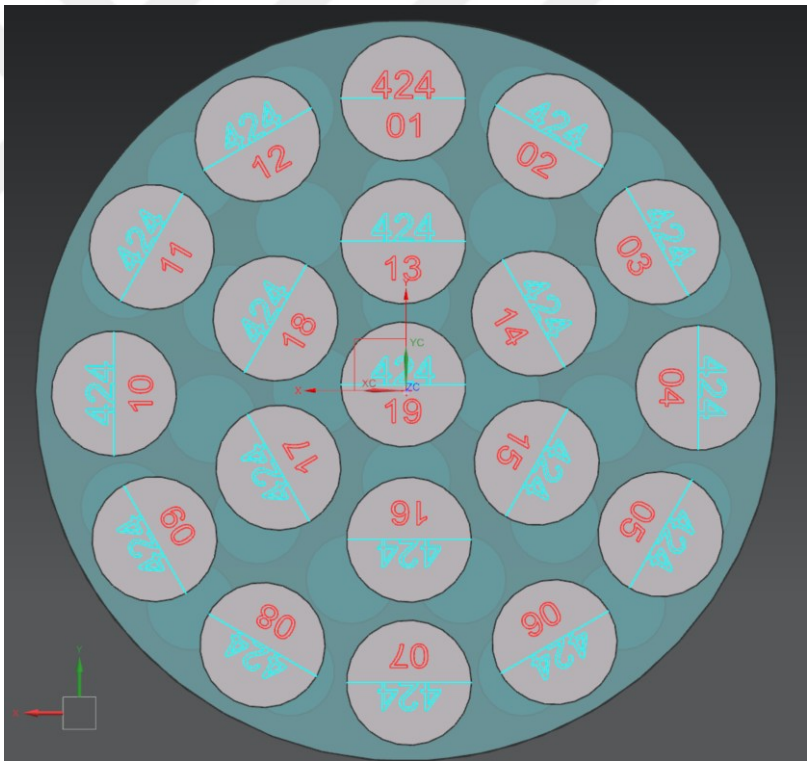

Figure 3.10. *Placement and identification of samples used for HCF testing within the billet*

Table 3.4. *Identification of samples used for the HCF test*

Sample code shown in Figure 3.10	Designation of scrap sample	Designation of virgin sample
3	HCF_1_S	HCF_1_V
5	HCF_2_S	HCF_2_V
6	HCF_3_S	HCF_3_V
13	HCF_4_S	HCF_4_V
15	HCF_5_S	HCF_5_V
16	HCF_6_S	HCF_6_V

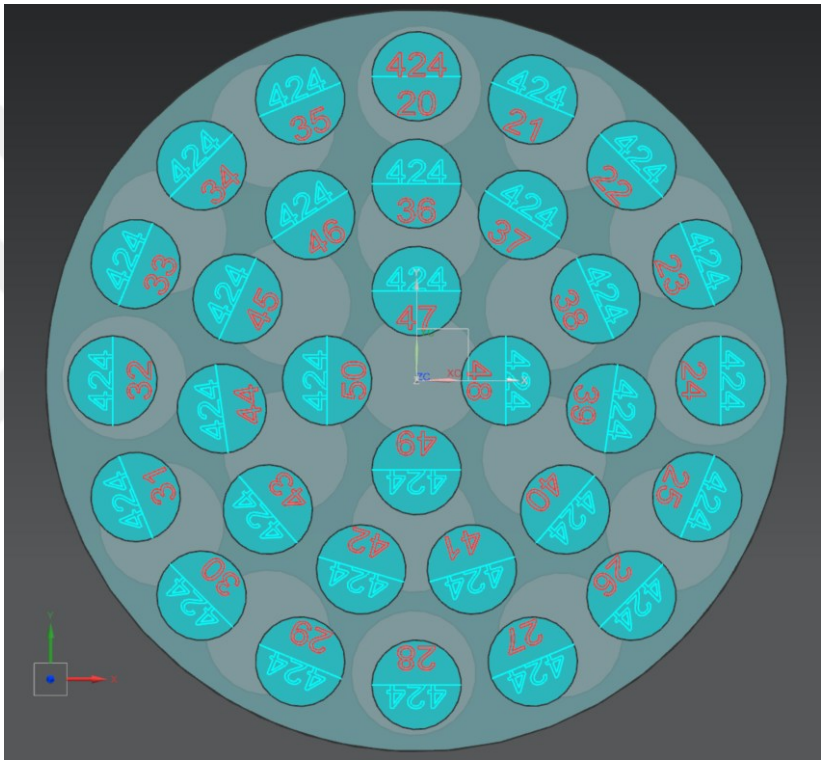

Figure 3.11. *Placement and identification of samples used for RT tensile, ET tensile, and stress-rupture tests within the billet*

Table 3.5. *Identification of samples used for RT tensile, ET tensile, and stress-rupture tests*

Sample code shown in Figure 3.11	Designation of scrap sample	Designation of virgin sample
28	RT_1_S	RT_1_V
29	RT_2_S	RT_2_V
31	RT_3_S	RT_3_V
32	RT_4_S	RT_4_V
33	RT_5_S	RT_5_V
42	RT_6_S	RT_6_V
44	RT_7_S	RT_7_V
45	RT_8_S	RT_8_V
50	RT_9_S	RT_9_V
35	ET_1_S	ET_1_V
36	ET_2_S	ET_2_V
37	ET_3_S	ET_3_V
46	ET_4_S	ET_4_V
47	ET_5_S	ET_5_V
26	SR_1_S	SR_1_V
39	SR_2_S	SR_2_V
48	SR_3_S	SR_3_V

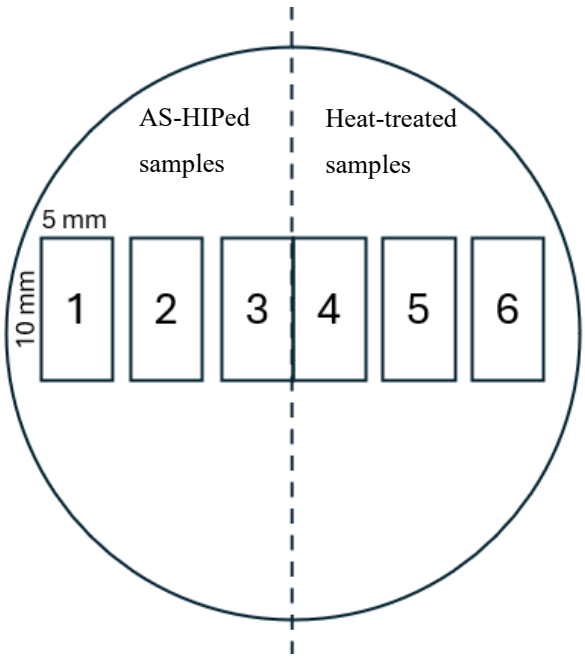

Figure 3.12. *Placement and identification of as-HIPed and heat-treated samples used for Archimedes, SEM, and microhardness analyses within the billet*

Table 3.6. *Identification of samples used for Archimedes, SEM, and microhardness analyses*

Sample code shown in Figure 3.12	Designation of scrap sample	Designation of virgin sample
1	1_S	1_V
2	2_S	2_V
3	3_S	3_V
4	4_S	4_V
5	5_S	5_V
6	6_S	6_V

3.1.7. Heat treatment

Solution and aging heat treatments were applied to the blanks extracted by EDM in accordance with the SAE/AMS Standard 5663 material specification, utilizing an atmospheric furnace. During the solution treatment, the samples were heated to 954°C, held at this temperature for 60 minutes, and then air cooled.

For the precipitation (aging) treatment, the material was first heated to 720°C and held for 490 minutes, followed by cooling at a rate of 56°C/h to 621°C, where it was maintained for 18 hours prior to final air cooling. The complete heat treatment cycle is depicted in Figure 3.13.

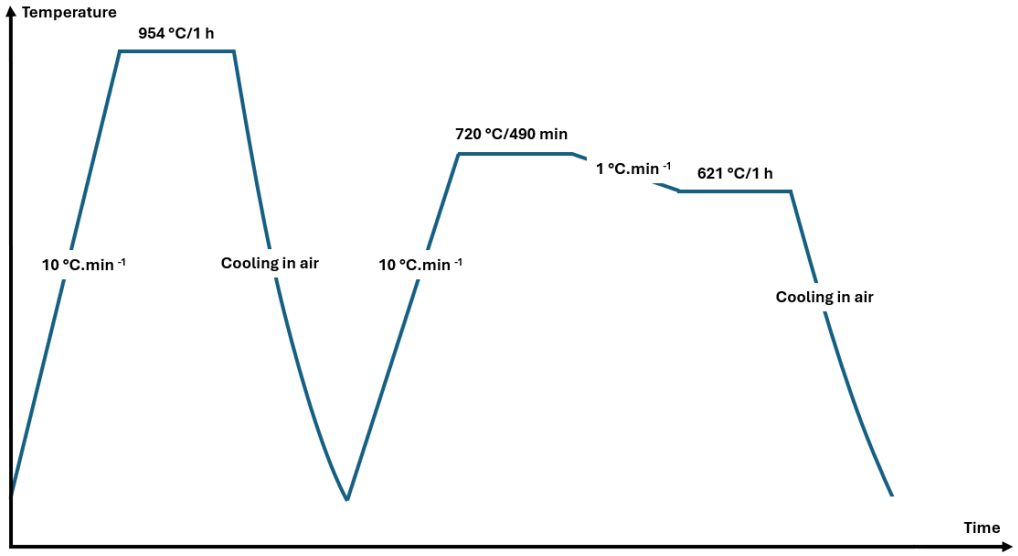

Figure 3.13. *Heat treatment cycle chart*

3.1.8. Machining of heat-treated samples to test geometries

Following the completion of the solution and aging heat treatments, the blank samples were machined by turning into dog bone geometries with dimensions suitable for HCF, room temperature tensile (RT), elevated temperature tensile (ET), and stress-rupture testing.

3.2. Characterization Techniques

In the following subsections, the characterization studies carried out on both virgin and scrap Inconel 718 powders used as feedstock materials, as well as on the sintered specimens produced from these powders, are presented.

3.2.1. Characterization of virgin and scrap Inconel 718 powders

In the following subsections, the characterization studies performed on virgin and scrap Inconel 718 powder feedstocks are described in detail.

3.2.1.1. *Scanning electron microscopy (SEM)*

The morphological features of the powder samples mounted on carbon tape were examined using SEM-SE imaging, while their surface textures were analyzed using SEM-SE.

3.2.1.2. *X-ray fluorescence (XRF)*

XRF analyses were conducted to determine the elemental composition of the virgin and scrap Inconel 718 powders.

3.2.1.3. *X-ray diffraction (XRD)*

XRD analyses were carried out to identify the phases present in the virgin and scrap Inconel 718 powders. The powder was scanned over a 2θ range of 30° to 100°, using a step size of 0.02° and a scan rate of 1°/min. Phase identification was accomplished by matching the raw data through interpolation.

3.2.1.4. *O/N elemental analysis*

The oxygen (O) and nitrogen (N) contents of both the virgin and scrap Inconel 718 powders were precisely measured via O/N elemental analysis in a helium (He) atmosphere, in accordance with ASTM E1019. During the analysis, the samples are melted in a ceramic crucible under an inert gas atmosphere. Under these conditions, oxygen is released as CO or CO_2, while nitrogen is released in the form of N_2. The oxygen content is quantified using an infrared detector, whereas the nitrogen content is measured with a thermal conductivity detector.

3.2.1.5. *Flow behavior*

To assess the flow characteristics of the virgin and scrap Inconel 718 powders, apparent density tests were performed following ASTM B212, tap density measurements according to ASTM B527, and flow rate analyses as per ASTM B213. The Hausner ratio was calculated by dividing the tap density by the apparent density.

3.2.1.6. *Particle size distribution*

The particle size distributions of the virgin and scrap Inconel 718 powders were determined by laser diffraction in accordance with ASTM B822, while sphericity was evaluated through image analysis.

3.2.2. Characterization of sintered samples produced from virgin and scrap Inconel 718 powders

In the following subsections, the characterization studies carried out on the sintered specimens produced from virgin and scrap Inconel 718 powders are described in detail.

3.2.2.1. *Archimedes density*

Archimedes principle, in accordance with ASTM B311, was employed to determine the density of the bulk samples that had been extracted from the billets, as illustrated in Figure 3.12 and detailed in Table 3.6. Each measurement was repeated three times to ensure accuracy and repeatability.

3.2.2.2. *Hardness test*

The hardness of the samples was evaluated by Brinell macrohardness testing in accordance with ASTM E10. This testing was conducted on the bulk samples documented in Figure 3.12 and Table 3.6, using a 187.5 kgf load with a 2.5 mm diameter indenter, and each measurement was repeated three times for consistency.

3.2.2.3. *Optical light microscopy*

Optical microscopy was performed to examine the microstructure of the produced samples. The surfaces of the bulk samples, which are shown in Figure 3.12and identified in Table 3.6, were polished and analyzed for optical porosity. Images were captured specifically from areas exhibiting the highest porosity, and the pore areas were quantified relative to the total inspected area.

3.2.2.4. *Scanning electron microscopy (SEM)*

Further microstructural characterization was conducted using SEM. The same bulk samples shown in Figure 3.12 and listed in Table 3.6 were first mechanically polished and then etched for 20 seconds in a solution containing 45% HCl, 45% methanol, and 10% H_2O_2. These SEM analyses facilitated the identification of precipitates, the assessment of porosity, and the detection of microstructural defects.

3.2.2.5. *X-ray diffraction (XRD)*

XRD analyses were carried out to identify the phases present in the produced samples. The polished surfaces of the bulk samples, whose details are provided in Figure 3.12 and Table 3.6, were scanned over a 2θ range of 30° to 80°, using a step size of 0.02° and a scan rate of 1°/min. Phase identification was accomplished by matching the raw data through interpolation.

3.2.2.6. *O/N elemental analysis*

The oxygen (O) and nitrogen (N) contents of the produced samples were precisely measured via O/N elemental analysis in a helium (He) atmosphere, in accordance with ASTM E1019. During the analysis, the samples are melted in a ceramic crucible under an inert gas atmosphere. Under these conditions, oxygen is released as CO or CO_2, while

nitrogen is released in the form of N_2. The oxygen content is quantified using an infrared detector, whereas the nitrogen content is measured with a thermal conductivity detector.

3.2.2.7. *Arc/spark optical emission spectrometry*

The chemical composition of the produced samples was precisely determined by performing Arc/Spark Optical Emission Spectrometry on the bulk samples extracted from the billets, as indicated in Figure 3.12 and described in Table 3.6. When a high energy electric arc is generated between the electrode and the conductive sample, material from the sample surface undergoes localized evaporation. The vaporized atoms emit radiation at characteristic wavelengths, which are then collected and analyzed by the spectrometer. By measuring the intensity of these emitted spectral lines, the specific elements present in the sample can be accurately identified.

3.2.2.8. *Room temperature tensile test*

Room temperature tensile tests were performed to assess the mechanical properties of the samples, following ASTM E8/E8M. The samples, which were prepared from the billets shown in Figure 3.11 and listed in Table 3.5, were tested under strain control at a rate of 0.5%/min up to the yield point. Beyond yielding, the tests continued under crosshead control at a speed corresponding to 0.05 times the reduced section length per minute. Elongation was measured in accordance with the 4B rule.

3.2.2.9. *Elevated temperature tensile test*

To evaluate high-temperature mechanical performance, elevated temperature tensile tests were conducted at 649°C in line with ASTM E21. The samples, prepared from the billets depicted in Figure 3.11 and identified in Table 3.5, were subjected to the same loading regime as at room temperature: strain-controlled at 0.5%/min up to yielding, followed by crosshead-controlled testing at 0.05 times the reduced section length per minute. Elongation was again determined using the 4B method.

3.2.2.10. *High cycle fatigue test*

High cycle fatigue tests were conducted in accordance with ASTM E466 on samples that were extracted from the produced billets, with their locations illustrated in

Figure 3.10 and their identifiers provided in Table 3.4. The samples were subjected to predefined stress levels of 300, 450 and, 650 MPa under 650 °C and testing was continued until either failure occurred or the sample demonstrated infinite fatigue life.

3.2.2.11. *Stress-rupture test*

Stress-rupture tests were performed to determine the high-temperature service life of the samples, following ASTM E139. These tests were carried out on the samples extracted from the billets shown in Figure 3.11 and detailed in Table 3.5. During testing, the specimens were heated to a target temperature of 649 °C and then subjected to constant stress levels of 550, 600, and 650 MPa. Once the target temperature had been reached, the applied stress was maintained, and the specimens were held under constant thermal and loading conditions until fracture occurred.

4. RESULT AND DISCUSSION

In the following subsections, the outcomes of the characterization studies carried out on virgin and scrap Inconel 718 powders, as well as on the sintered specimens produced from these powders, are presented.

4.1. Characterization of Virgin and Scrap Inconel 718 powders

The specifics and outcomes of the characterization analyses conducted on the virgin and scrap Inconel 718 powders employed as raw materials are provided in the following subsections.

4.1.1. Scanning electron microscopy (SEM)

The morphological features and surface textures of the powder samples mounted on carbon tape were analyzed using secondary electron imaging in scanning electron microscopy (SEM-SE). The findings for both the virgin and scrap Inconel 718 powders are presented in Figure 4.1.

SEM-SE micrographs indicate that both powder types predominantly exhibit spherical morphologies, although a small fraction of particles display irregular shapes. Even a minor presence of such irregularly shaped particles can increase interparticle friction and mechanical interlocking, thereby impeding the free flow of the powders.

In the scrap Inconel 718 powder, a greater degree of satellite formation was observed, along with noticeably rougher particle surfaces. Both increased satellites and surface roughness are expected to elevate frictional forces and enhance mechanical interlocking during powder flow, ultimately reducing flowability. Moreover, powders characterized by pronounced satelliting and rough surfaces are less likely to achieve optimal packing during sintering, as these particles cannot readily rearrange and fill void spaces, which may adversely affect final densification.

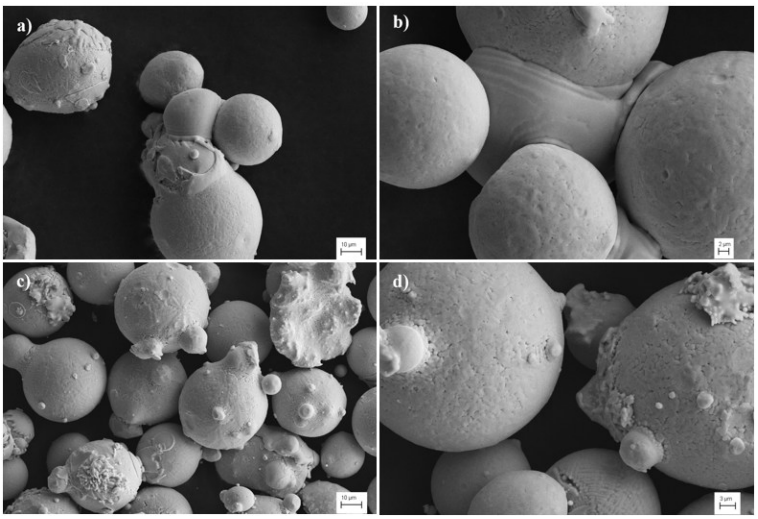

Figure 4.1. *SEM-SE micrographs at various magnifications showing (a, b) virgin Inconel 718 powders and (c, d) scrap Inconel 718 powders*

4.1.2. X-ray fluorescence (XRF)

The elemental compositions of the virgin and scrap Inconel 718 powders were analyzed using X-ray fluorescence (XRF), with the results summarized in Table 4.1. The data indicate that the titanium content in the scrap Inconel 718 powder falls outside the specified range of 0.65–1.15 wt.% established by ASTM F3055 and shown in *Table **2.1***. This deviation from the standard chemical composition confirms that the powder is correctly classified as scrap.

Table 4.1. *XRF analysis results detailing the elemental compositions of the virgin and scrap Inconel 718 powders*

Element	Virgin Inconel 718	Scrap Inconel 718
Ni (wt.%)	52.45 ± 0.042	52.52 ± 0.014
Cr (wt.%)	19.50 ± 0.014	18.78 ± 0.042
Fe (wt.%)	18.74 ± 0.028	19.15 ± 0.014
Nb (wt.%)	4.90 ± 0.057	5.12 ± 0.028
Mo (wt.%)	3.01 ± 0.057	3.13 ± 0.014
Ti (wt.%)	0.84 ± 0.014	0.54 ± 0.028
Al (wt.%)	0.31 ± 0.071	0.34 ± 0.014
Mn (wt.%)	0.25 ± 0.042	0.28 ± 0

4.1.3. X-ray diffraction (XRD)

XRD analysis of both virgin and scrap Inconel 718 powders, as shown in Figure 4.2, revealed that the dominant alloy phase present was the γ-phase, characterized by a nickel-based FCC crystal structure. XRD examination of the material did not reveal any other distinct phases. This was primarily due to the challenges in distinguishing diffraction peaks in the diffractograms, compounded by the limited phase identification data available in the literature and the constraints of the reference database.

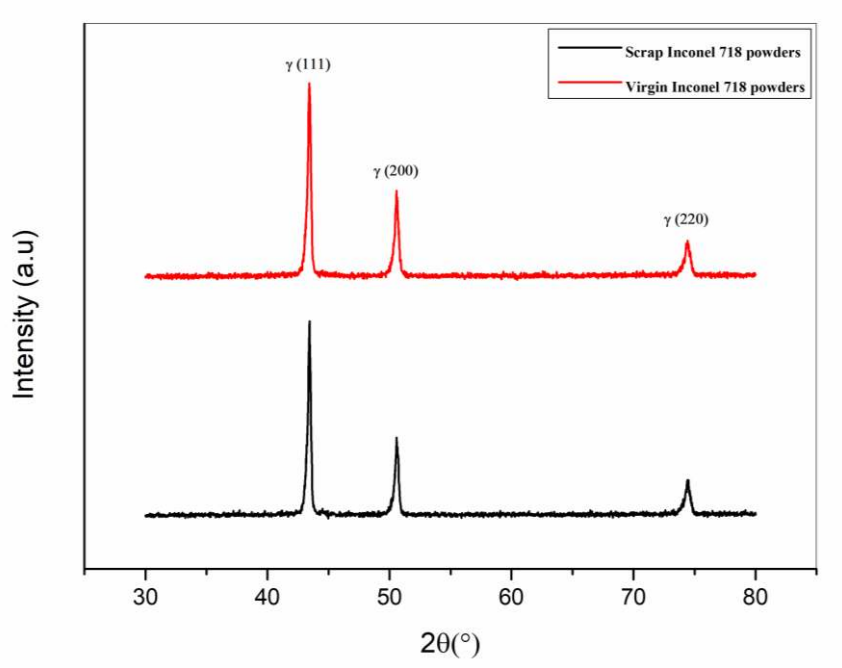

Figure 4.2. *XRD Analysis results of the virgin and scrap Inconel 718 powders*

4.1.4. O/N elemental analysis

Elevated oxygen and nitrogen levels are known to facilitate the formation of oxide and nitride phases, which can disrupt the desired phase distribution and give rise to detrimental phases that impair mechanical properties such as elongation and creep resistance [46-47]. To assess this, O/N elemental analysis was performed to quantify the oxygen and nitrogen contents in the virgin and scrap Inconel 718 powders, with the results summarized in Table 4.2.

Although ASTM F3055 does not specify explicit limits for oxygen and nitrogen, it underscores that their concentrations should be controlled to avoid compromising mechanical performance. Literature surveys generally recommend maintaining the

combined oxygen and nitrogen content below 300 ppm to achieve optimal material behavior. The analysis results show that both powders possess O and N levels within acceptable limits, indicating their suitability in this regard.

Table 4.2. *O/N elemental analysis results for the virgin and scrap Inconel 718 powders*

Element	Virgin Inconel 718	Scrap Inconel 718
O (ppm)	107.81 ± 16.77	124.05 ± 6.72
N (ppm)	90.32 ± 0.45	84.36 ± 6.70

4.1.5. Flow behavior

To assess the flow characteristics of the virgin and scrap Inconel 718 powders, measurements were conducted to determine their apparent density, tap density, flow rate, and Hausner ratio. The results are presented in
Table 4.3. Analysis of the data indicates that the morphology of the scrap powder does not negatively impact its apparent or tap density. Additionally, the Hausner ratios and flow rates for both the virgin and scrap powders are quite similar, with nearly all values falling within the range typically categorized as “good,” thereby reflecting satisfactory flowability.

Table 4.3. *Flow behavior analysis results for virgin and scrap Inconel 718 powders*

Properties	Virgin Inconel 718		Scrap Inconel 718	
Appearent Density (g/cc)	4.515 ± 0.027		4.465 ± 0.020	
Tap Density (g/cc)	5.320 ± 0.058		5.103 ± 0.001	
Flow Rate (sec)	16.03 ± 0.21		16.7 ± 0.1	
Hausner Ratio	1.18	Good	1.14	Good

4.1.6. Particle size distribution

The particle size distribution (PSD) and sphericity values for the virgin and scrap Inconel 718 powders are summarized in Table 4.4. According to the literature, achieving optimal packing behavior generally requires powder sizes to fall within the 20 to 45 μm range. The analysis reveals that the extensive satelliting present in the scrap powder notably increases its D90 value and negatively impacts particle sphericity. In contrast, the

D90 of the virgin powder is substantially lower and closely aligns with the recommended range, indicating superior packing characteristics relative to the scrap powder.

Moreover, the relatively low sphericity of the scrap powder is expected to elevate interparticle friction and encourage mechanical interlocking. The increased surface area of non-spherical particles also enhances cohesion, resulting in stronger particle adhesion and diminished free flowability. Additionally, because irregularly shaped particles tend to pack less efficiently, they introduce voids within the powder bed, which can ultimately lead to reduced densities in the final fabricated components.

Table 4.4. *Particle size distribution and sphericity measurements for virgin and scrap Inconel 718 powders*

Properties	**Virgin Inconel 718**		**Scrap Inconel 718**	
Size (µm)	D10	24.38 ± 0.95	D10	24.02 ± 0.86
	D50	36.13 ± 0.52	D50	35.73 ± 1.13
	D90	47.09 ± 2.86	D90	53.22 ± 1.96
Sphericity (%)	>0.5	99.93	>0.5	100
	>0.7	99.24	>0.7	96.85
	>0.9	90.27	>0.9	77.40

4.2. Characterization of Sintered Samples Produced from Virgin and Scrap Inconel 718 Powders

The specifics and outcomes of the characterization analyses conducted on the sintered samples produced from virgin and scrap Inconel 718 powders are provided in the following subsections.

4.2.1. Archimedes density

Archimedes density measurements were performed to assess the relative densities of both heat-treated and as-HIPed samples, with the results summarized in Table 4.5. The data indicate that the satelliting and pronounced surface roughness of the scrap Inconel 718 powders adversely affected their packing efficiency, leading to bulk samples with lower densities compared to those produced from virgin powders. Archimedes density measurements showed that areas of the billet which first came into contact with temperature and pressure during the HIP process had higher density values than those at the capsule's center. This suggests that heat and pressure are transferred more efficiently to the outer regions, while consolidation in the central zone remains less complete.

Increased porosity within the structure can act as a site for localized stress concentrations, thereby facilitating crack initiation. This is particularly concerning under high-temperature and long-duration loading conditions, where creep and fatigue resistance are critical and may be significantly degraded. Moreover, materials with elevated porosity generally exhibit reduced elongation, shifting their fracture behavior toward a more brittle failure mode.

Additionally, the phase transformations and relief of internal stresses occurring during heat treatment contributed to the formation of microvoids, resulting in a general decrease in the densities of all heat-treated samples relative to their as-HIPed counterparts. Moreover, thermally induced porosity is among the most critical defects encountered in powder metallurgy superalloys. The proportion of such pores tends to rise with increasing temperature or extended holding time. This defect is generally attributed to three primary causes. The first reason is hollow powder particles, likely formed during argon atomization, may trap insoluble gases, which expand during heat treatments after HIP and generate isolated pores within the material. The second is insoluble gases adsorbed on the surface of the powder may not be completely eliminated during evacuation, leaving residual gases that can promote pore formation. And the last one is if the container experiences any leakage during HIP, inert gas can infiltrate the powder, leading to gas-filled porosity [49].

Table 4.5. *Archimedes density results for as-HIPed and heat-treated samples*

Heat Treatment Conditions	**Properties**	**Virgin Inconel 718**			**Scrap Inconel 718**		
	Sample Name	1_V	2_V	3_V	1_S	2_S	3_S
No	Archimedes Density (g/cc)	8.192 ± 0.002	8.182 ± 0.003	8.171 ± 0.006	8.015 ± 0.001	7.950 ± 0.001	7.910 ± 0.002
	Relative Density (%)	99.66	99.54	99.4	97.51	96.72	96.23
	Sample Name	4_V	5_V	6_V	4_S	5_S	6_S
Yes	Archimedes Density (g/cc)	8.151 ± 0.001	8.156 ± 0.003	8.168 ± 0.003	7.679 ± 0.009	7.730 ± 0.003	7.871 ± 0.002
	Relative Density (%)	99.16	99.22	99.37	93.42	94.04	95.75

4.2.2. Hardness test

Brinell macrohardness tests were performed to evaluate the hardness of both as-HIPed and heat-treated samples, with the results summarized in Table 4.6. In the as-HIPed samples, macrohardness values were found to decrease progressively from regions of relatively higher to lower density. This trend aligns with the understanding that pores within the structure hinder the effective transmission of applied loads, resulting in greater indentation depths and consequently lower hardness readings in less dense areas.

Additionally, the phase transformations and relief of residual stresses by heat treatment promoted the formation of microvoids, which reduced the overall density of the samples and led to further decreases in macrohardness. Despite these reductions, it is noteworthy that all samples satisfied the minimum hardness requirement of 331 HB as specified in SAE/AMS Standard 5663.

Table 4.6. *Brinell macrohardness measurements for as-HIPed and heat-treated samples*

Heat Treatment Conditions	**Properties**	**Virgin Inconel 718**			**Scrap Inconel 718**		
	Sample Name	1_V	2_V	3_V	1_S	2_S	3_S
No	HB	432.33 ± 6.34	430 ± 19	415 ± 0	393 ± 17.78	368.3 ± 4.62	358.3 ± 4.04
	Sample Name	4_V	5_V	6_V	4_S	5_S	6_S
Yes	HB	413 ± 0	410 ± 5.20	409.67 ± 5.77	400.67 ± 5.77	386.33 ± 7.03	376.33 ± 9.25

4.2.3. Optical light microscopy

Optical light microscopy was utilized to capture porosity images of the fabricated samples and to quantify the ratio of total pore area to the overall sample area, with the results presented in Figure 4.3 and Figure 4.4. Analysis of the data reveals that samples produced from virgin Inconel 718 powders exhibited lower porosity levels compared to those manufactured using scrap powders. Furthermore, an increase in porosity was noted after the application of heat treatment. Importantly, the porosity values determined through optical analysis were in good agreement with the trends observed in the Archimedes density measurements.

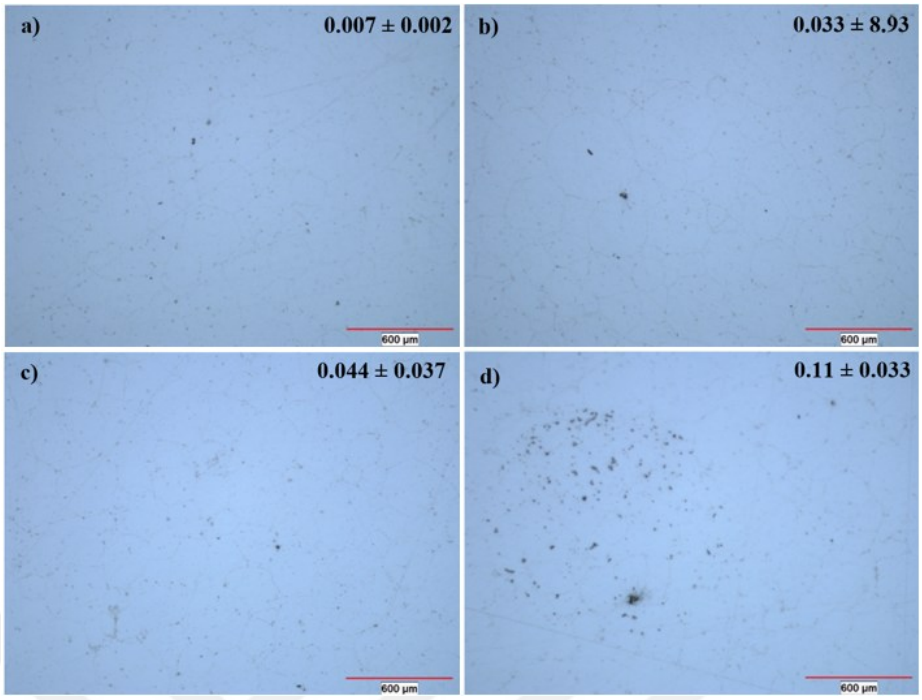

Figure 4.3. *Optical porosity results of as-HIPed samples a) 1_V, b) 3_V, c)1_S, and d) 3_S*

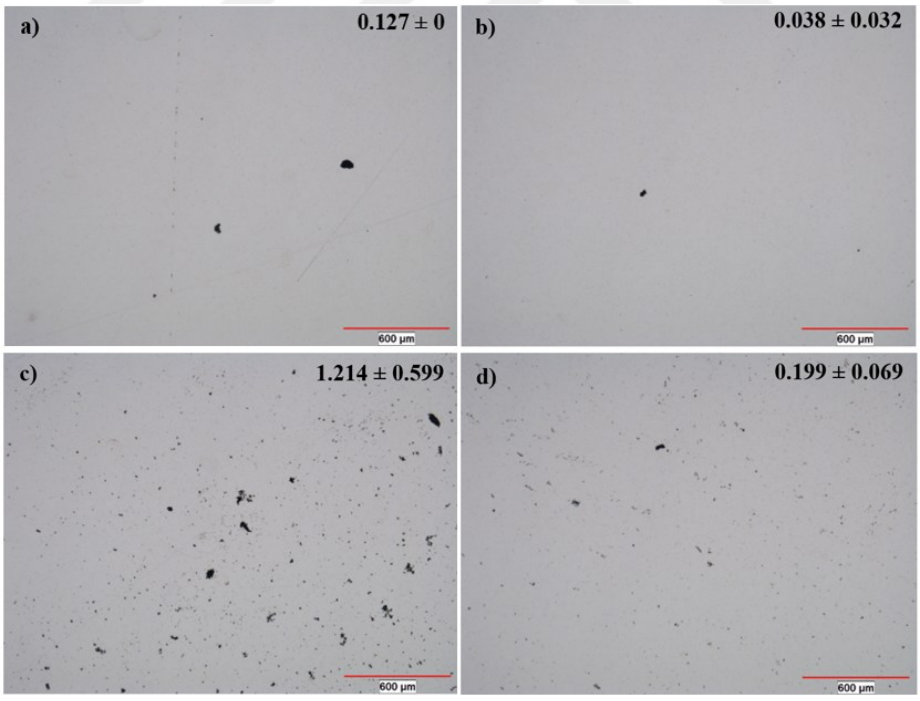

Figure 4.4. *Optical porosity results of as-HIPed samples a) 4_V, b) 6_V, c)4_S, and d) 6_S*

4.2.4. Scanning electron microscopy (SEM)

SEM-SE micrographs of the polished samples clearly highlight the distribution, size, and frequency of pores within the microstructure. In sections Figure 4.5 and Figure

4.6, the 1_V and 6_V samples, as well as the 1_S and 6_S samples, positioned in areas that are first exposed to pressure and temperature during the HIP cycle, display smaller and fewer pores. By contrast, the 3_V and 4_V samples, along with the 3_S and 4_S samples, taken from regions nearest to the capsule center, show a greater number of pores, many of which are larger in size. These microstructural observations are in agreement with the density values obtained from Archimedes measurements and the porosity assessments from optical microscopy.

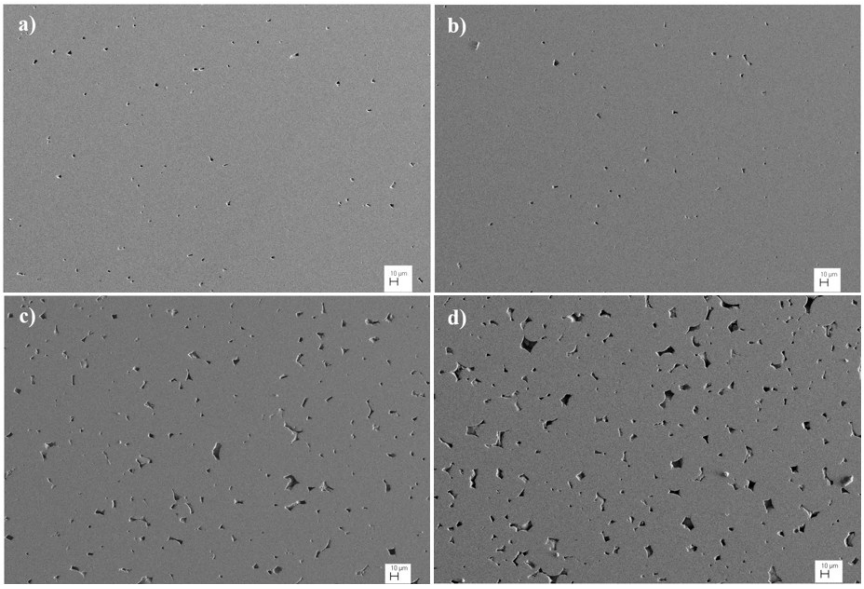

Figure 4.5. *SEM-SE micrographs of as-HIPed samples a) 1_V, b) 3_V, c)1_S, d) 3_S*

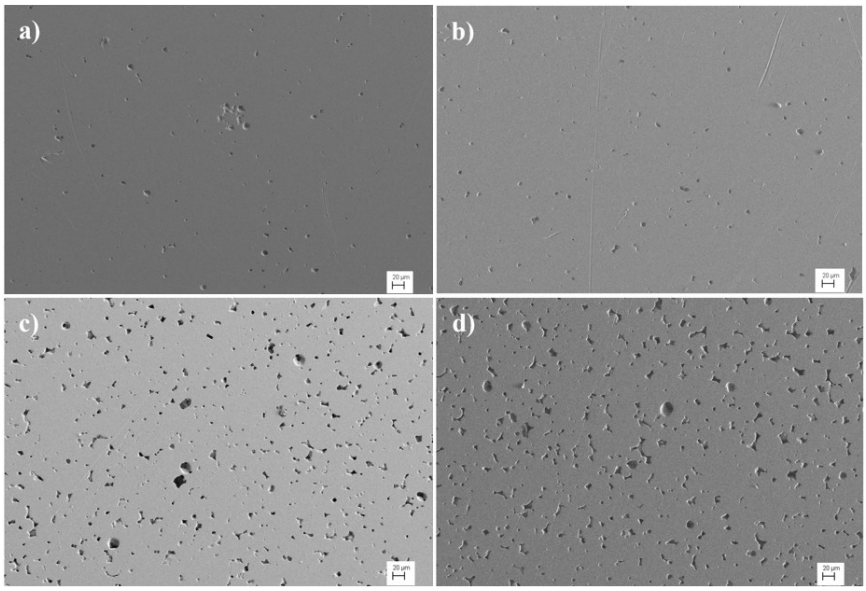

Figure 4.6. *SEM-SE micrographs of the heat-treated samples a) 4_V, b) 6_V, c)4_S, d) 4_S*

SEM-EDX analyses were performed on both etched and unetched samples in the as-HIPed and heat-treated conditions, produced from virgin and scrap Inconel 718 powders. The findings regarding chemical composition and precipitate distribution are summarized below.

In Figure 4.7, Figure 4.9, Figure 4.11, and Figure 4.13, the unetched specimens exhibit weak image contrast, which makes phase identification more difficult compared to the etched specimens shown in Figure 4.8, Figure 4.10, Figure 4.12, and Figure 4.14.

For this reason, the interpretation of phases within the microstructure was based on both the morphological features of the regions from which spectrum were collected and their corresponding elemental compositions. The combined SEM-EDX observations from Figure 4.7 through Figure 4.14 indicate the following:

- The γ (gamma) matrix consistently appears as a medium-gray background in all microstructures and serves as the reference tone.
- γ′ (gamma prime) and γ″ (gamma double prime) cannot be resolved by SEM due to their nanometric size.
- The δ (delta) phase, with a higher average atomic number than the γ matrix, is identified by its bright contrast and characteristic needle-like morphology.
- The Laves phase, also richer in heavy elements than the γ matrix, appears brighter and exhibits irregular morphologies.
- Metal carbides generally appear darker relative to the matrix, although those with higher metallic content may display brighter contrast.
- Nitride- and oxide-based precipitates, due to their lower average atomic numbers, typically appear darker than the surrounding matrix.
- It was also observed that the heat-treated specimens contained a noticeably higher density of precipitates in their microstructures compared with the as-HIPed counterparts. Moreover, the precipitates in the etched samples were more distinctly resolved, allowing for clearer identification, whereas those in the unetched specimens were more difficult to distinguish.

When examining the SEM-EDX results of the unetched, as-HIPed samples produced from virgin Inconel 718 powders shown in Figure 4.7. In spectrum 1 (a-1) corresponds to an intragranular and homogeneous area situated on a gray background. The strongest peak is attributed to Ni, confirming its role as the primary element of the γ matrix. The notable presence of Cr and Fe further supports this interpretation. The

detected carbon signal, however, is likely due to contamination from the Bakelite mounting resin rather than the presence of carbides, as no morphological evidence or localized metallic enrichment characteristic of carbide precipitates was observed in the microstructure. It is possible that Bakelite penetrated into pores during sample preparation, which in turn may have caused an artificially elevated carbon reading within the interaction volume. The moderate Nb content and the low Al content indicate that these elements are probably retained in solid solution within the surrounding matrix.

In spectrum 1 (b-1), the elemental profile shows high concentrations of Ni, Fe, and Cr. While these values are generally characteristic of the γ matrix, the spot analyzed actually corresponds to a very small, dark-contrast precipitate. Because of the tiny size of this feature relative to the much larger interaction volume, the detected peaks are partially influenced by elements from the surrounding matrix. Compared with region a-1, the C level in (b-1) is higher, and the moderate Nb signal suggests that this site may represent a NbC-type carbide.

In spectrum 1 (c-1), the Ni content is somewhat lower than in the other spectrums but still remains relatively high. The Cr level is greater than in (a-1) and (b-1), though it does not surpass Ni in dominance. A strong Nb peak is clearly visible, and unlike the other spectrums, Ti appears here in small amounts. C is also detected, though at lower levels compared with the other regions. The bright contrast observed in this area, combined with the pronounced Nb content, strongly suggests that the phase present is Laves. The additional contributions of Ni, Fe, and Cr can be explained by signals originating from the surrounding γ matrix within the interaction volume.

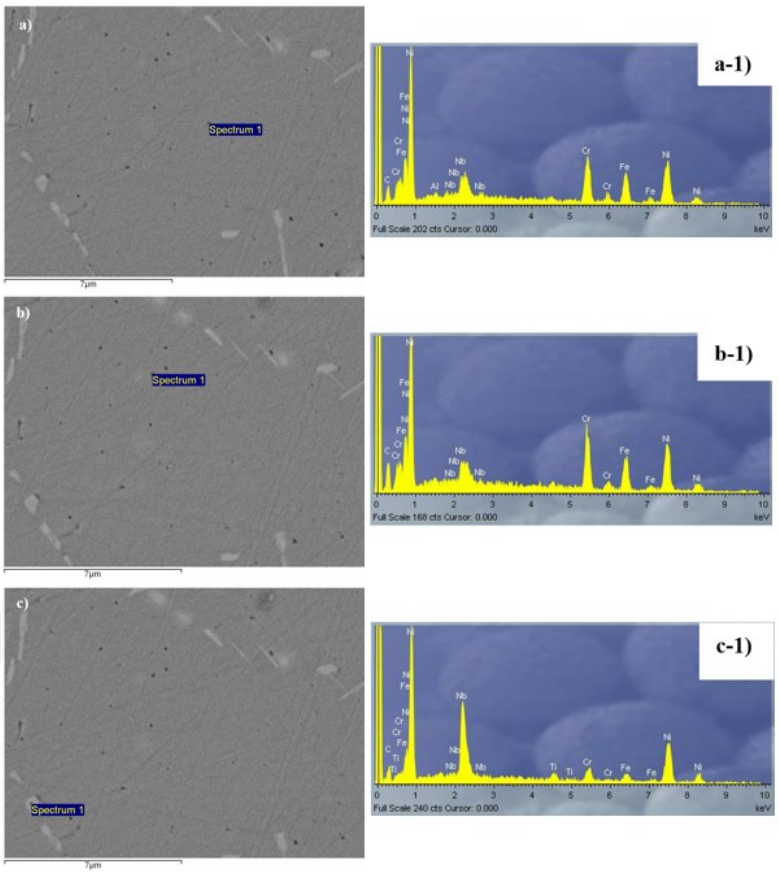

Figure 4.7. *SEM-EDX analysis results of non-etched as-HIPed sample 1_V*

When analyzing the SEM-EDX results of the etched, as-HIPed samples produced from virgin Inconel 718 powders shown in Figure 4.8. In Spectrum 1 (a-1), the analyzed region exhibits a bright contrast with angular morphology and contains high concentrations of Nb and Mo, along with moderate amounts of C, Ni, Fe, Cr, and Ti. While this chemical composition could correspond either to a carbide-based precipitate or to a Laves phase, the angular morphology and bright contrast suggest that it is more likely a Laves phase.

Spectrum 2 (a-2), based on its elemental composition, is identified as the γ matrix.

In Spectrum 1 (b-1), the analyzed region contains precipitates with a needle-like morphology and a brighter contrast than the surrounding matrix. The elemental composition indicates high concentrations of Ni, Fe, and Cr, together with moderate amounts of Nb, Mo, and Ti. Taking both the morphology and chemistry into account, these precipitates are identified as δ-phase. The contributions of Mo, Ni, Fe, and Cr are likely influenced by the interaction volume, reflecting overlap from the adjacent γ matrix and nearby precipitates.

Spectrum 2 (b-2), based on its elemental composition, is identified as the γ matrix.

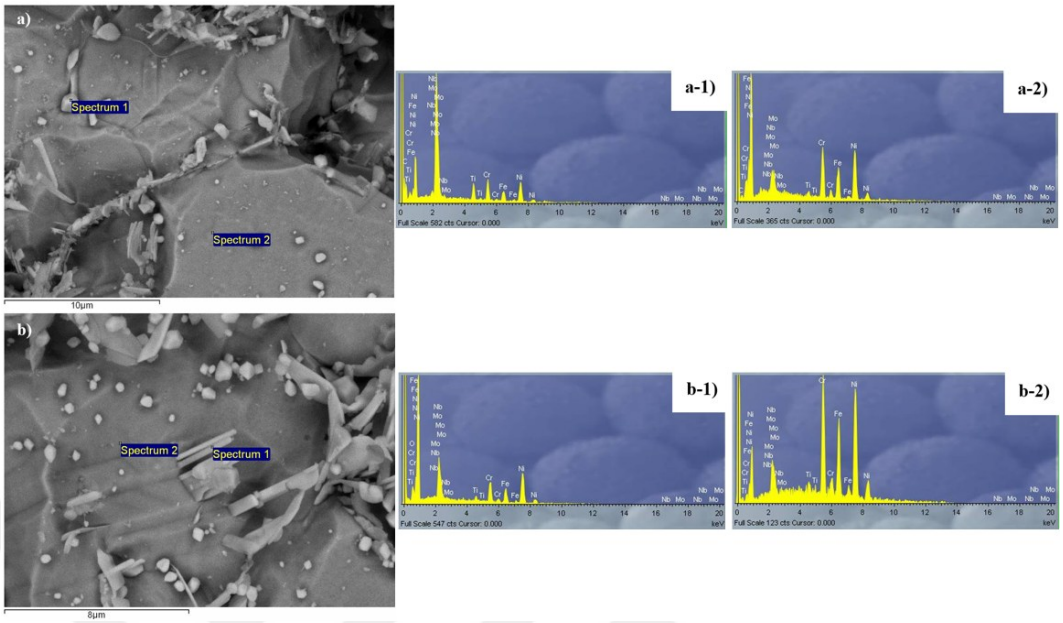

Figure 4.8. *SEM-EDX analysis results of etched as-HIPed sample 1_V*

When analyzing the SEM-EDX results of the unetched, as-HIPed samples produced from scrap Inconel 718 powders shown in Figure 4.9. In the area corresponding to Spectrum 1 (a-1), the dark contrast suggests that the region belongs to a precipitate with a relatively low atomic number. The spectrum shows pronounced Ni, Fe, and Cr peaks, accompanied by distinct Nb peaks and a strong C signal. The simultaneous detection of Nb and C points toward the presence of NbC. However, the unusually high C level compared to Nb also raises the possibility that this area represents a pore contaminated with C, with the Nb contribution coming from adjacent features within the interaction volume. The elevated Ni, Fe, and Cr levels can likewise be explained by signal overlap from the surrounding γ matrix or neighboring precipitates.

In Spectrum 2 (a-2), Nb is dominant and much higher than in (a-1), whereas Cr, Ti, and C are only detected in small amounts. Peaks for Ni and Fe, which would normally signify the γ matrix, are absent. This composition suggests the region corresponds to Laves phase. Spectrum 3 (a-3) was acquired from a gray, homogeneous region, consistent with the γ matrix, which is rich in Ni, Fe, and Cr. The Nb level is lower than in (a-2) but comparable to (a-1), and a small C signal is also present. This indicates that while the

region is largely γ matrix, Nb-containing precipitates or nearby carbide/pore features may also be contributing to the spectrum.

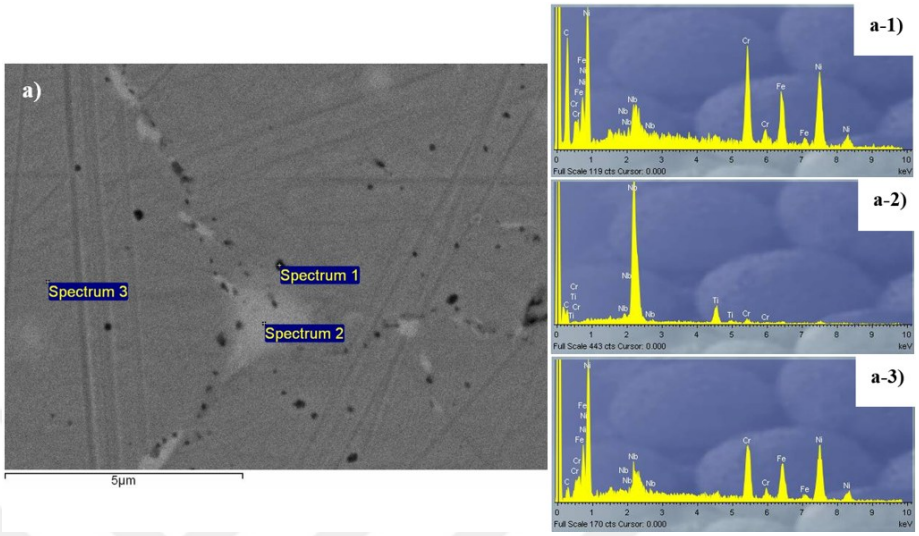

Figure 4.9. *SEM-EDX analysis results of non-etched as-HIPed sample 1_S*

When examining the SEM-EDX results of the etched, as-HIPed samples produced from scrap Inconel 718 powders shown in Figure 4.10. In Spectrum 1 (a-1), the examined region contains a bright-contrast, rod-like precipitate. The elemental analysis shows high levels of Ni, Fe, and Cr, with moderate amounts of Nb and Mo, and only low levels of C and Ti. Based on both morphology and composition, this precipitate is identified as δ-phase. The signals of Mo and Ti are most likely contributions from the interaction volume, while the small amount of carbon is attributed to contamination from the mounting material.

Spectrum 2 (a-2), based on its elemental composition, is identified as the γ matrix.

In Spectrum 1 (b-1), the analyzed region reveals a bright-contrast, angular precipitate. The chemical analysis shows high concentrations of Nb and Mo, together with moderate amounts of Ni, Fe, Cr, Ti, and C. Considering both the morphology and the composition, this precipitate is identified as a Laves phase.

Spectrum 2 (b-2), based on its elemental composition, is identified as the γ matrix.

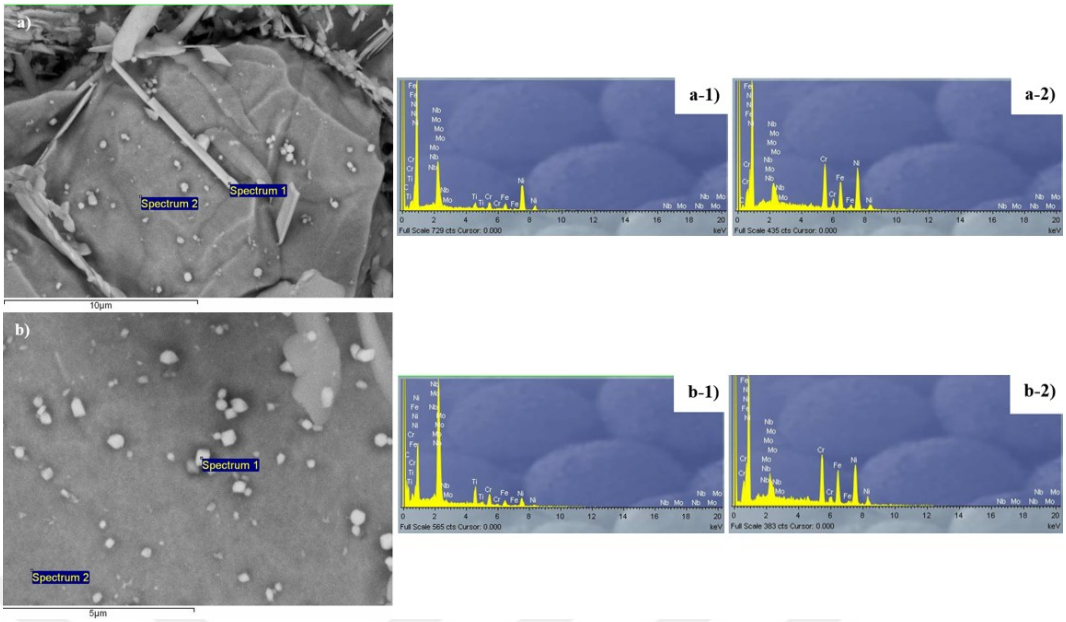

Figure 4.10. *SEM-EDX analysis results of etched as-HIPed sample 1_S*

When analyzing the SEM-EDX results of the unetched, heat-treated samples produced from virgin Inconel 718 shown in Figure 4.11. In Spectrum 1 (a-1), the region analyzed appears bright under SEM, suggesting the presence of elements with relatively high atomic numbers. The EDX results show Nb as the dominant element, with Ni, Fe, and Cr detected at moderate levels, and only a small amount of C. Ti is also present at a low level but still higher than the C content. The detected carbon could be related to contamination from the Bakelite mounting material used during preparation. Considering the bright contrast, along with the significant Nb and detectable Ti peaks, this region is most consistent with a Laves-type intermetallic phase. The contribution of Ni, Fe, and Cr is likely due to overlap from the surrounding γ matrix within the interaction volume.

Spectrum 2 (a-2), based on its elemental composition, is identified as the γ matrix.

In Spectrum 1 (b-1) spectrum was taken from a dark-contrast, angular precipitate. The results show high concentrations of Ni, Fe, and Cr, which at first glance suggest the γ matrix. However, given the relatively large interaction volume, these peaks are likely influenced by contributions from the surrounding material. The medium-to-low levels of Nb, Ti, and Al detected here indicate that the precipitate could correspond to an oxide- or nitride-based phase, which aligns with its dark contrast and angular morphology. Since oxygen and nitrogen peaks often occur at low energy, they may not be visible in the spectrum. The small amount of carbon detected is most likely an artifact of Bakelite contamination introduced during specimen preparation.

In Spectrum 2 (b-2), based on its elemental composition, is identified as the γ matrix.

In Spectrum 1 (c-1), the examined region displays a slender, rod-like precipitate with dark contrast. The dark appearance suggests that this phase contains elements with a lower average atomic number compared to the surrounding matrix. Its elongated, anisotropic morphology further indicates growth that is crystallographically less compatible with the γ matrix. Similar to the findings in (a-1), pronounced Nb peaks are visible in (c-1); however, in this case, Al, Ti, and O peaks also appear at relatively high levels. This combination strongly points to the presence of an oxide-based precipitate enriched in Nb, Al, and Ti. The small carbon signal detected is most likely due to contamination from the Bakelite mounting resin. Meanwhile, the medium-intensity Ni, Fe, and Cr peaks are interpreted as contributions from the surrounding γ matrix or from other nearby precipitates within the interaction volume.

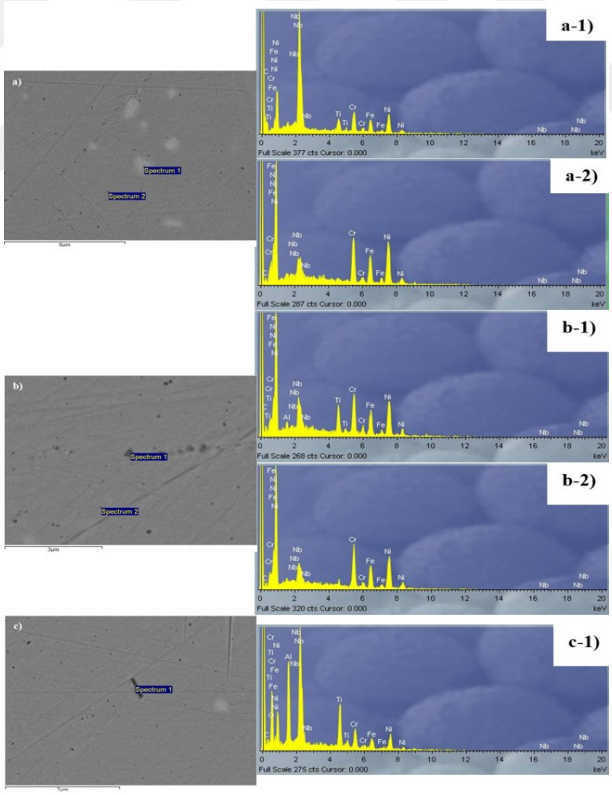

Figure 4.11. *SEM-EDX analysis results of non-etched heat-treated sample 6_V*

When analyzing the SEM-EDX results of the etched, heat-treated samples produced from virgin Inconel 718 powders shown in Figure 4.12. In Spectrum 1 (a-1), the analyzed

region contains a bright-contrast, angular precipitate. The composition shows high Nb and Mo contents, together with moderate amounts of Ni, Fe, Cr, and Ti. Based on both morphology and chemistry, this precipitate is identified as a Laves phase. The Ni, Fe, and Cr signals may originate directly from the precipitate but could also include contributions from adjacent phases or the surrounding γ matrix within the interaction volume.

Spectrum 2 (a-2), based on its elemental composition, is identified as the γ matrix.

In Spectrum 1 (b-1), the analyzed region shows very high Ni, Fe, and Cr contents, with moderate amounts of Nb and Mo, and small contributions from Al, Ti, and C. Because this spectrum was collected from a small precipitate, the strong Ni, Fe, and Cr signals are likely influenced by the surrounding γ matrix. Taking into account both the morphology and elemental composition, the precipitate is identified as a Laves phase. The low Al and Ti levels are probably contributions from dissolved elements in the nearby matrix or from adjacent precipitates within the interaction volume.

Spectrum 2 (b-2) based on its elemental composition, is identified as the γ matrix.

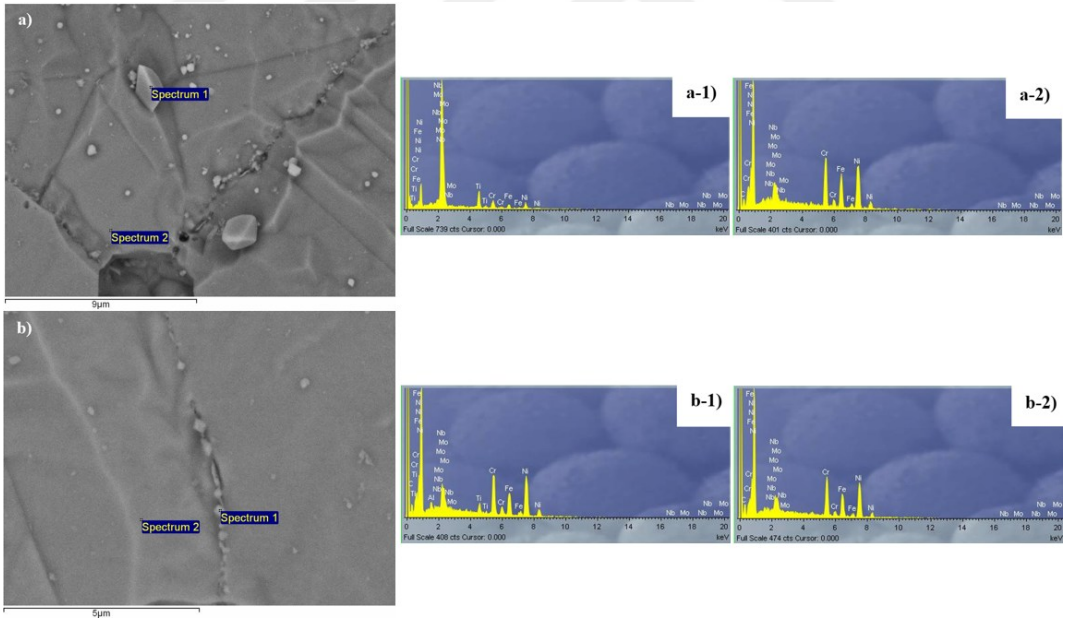

Figure 4.12. *SEM-EDX analysis results of etched heat-treated sample 6_V*

When examining the SEM-EDX results of the unetched, heat-treated samples produced from scrap Inconel 718 shown in Figure 4.13. In the region analyzed as Spectrum 1 (a-1), a bright-contrast phase is visible. Elemental analysis shows this area contains a very high concentration of Nb, a small amount of Ti, and low levels of Ni and Cr. The trace amount of C is most likely an artifact introduced by Bakelite contamination

during sample preparation. Given both the morphology and the chemical composition, and considering that the carbon level is too low to form carbide precipitates, this phase is most plausibly identified as a Laves phase.

In Spectrum 2 (a-2), based on its elemental composition, is identified as the γ matrix.

In Spectrum 1 (b-1), the examined region appears as a dark-contrast, angular precipitate. The elemental profile shows high Ni, Fe, and Cr levels, but these peaks are likely influenced by the relatively large interaction volume rather than the true composition of the precipitate. Alongside this, the spectrum reveals moderate carbon together with high Nb and moderate Ti contents, suggesting the presence of a complex NbC–TiC carbide phase. The weak sulfur peak detected is probably an overlap effect with Nb.

Spectrum 2 (b-2), based on its elemental composition, is identified as the γ matrix.

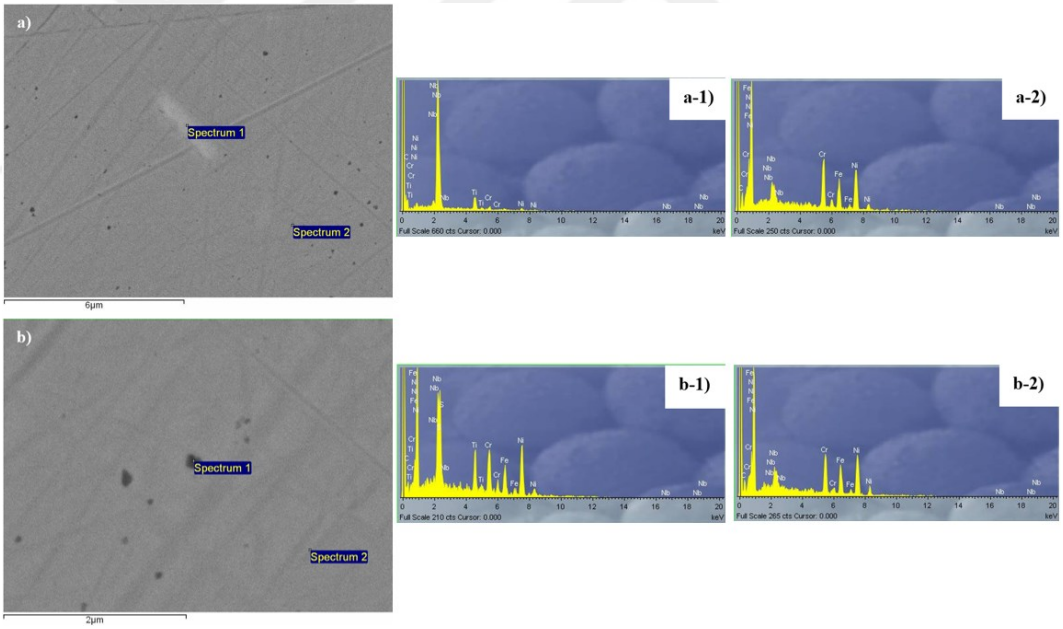

Figure 4.13. *SEM-EDX analysis results of non-etched heat-treated sample 6_S*

When examining the SEM-EDX results of the etched, heat-treated samples produced from scrap Inconel 718 powders shown in Figure 4.14. In Spectrum 1 (a-1), the analyzed region corresponds to a bright, angular precipitate containing high levels of Nb and Mo, along with moderate amounts of Ti and C, and lower levels of Ni, Fe, and Cr.

Considering both morphology and chemical composition, this precipitate is interpreted as a Laves phase.

Spectrum 2 (a-2), based on its elemental composition, is identified as the γ matrix.

In Spectrum 3 (a-3), the examined region shows a porous, gray, homogeneous background. It contains high Ni, Cr, and Fe levels, with moderate Ti, Nb, and Mo. The dominant Ni, Fe, and Cr levels identify this area as the γ matrix, while the additional Ti, Nb, and Mo may result either from elements dissolved in the matrix or from contributions of nearby precipitates within the interaction volume. The very low carbon signal is most likely due to Bakelite contamination introduced during sample preparation.

In Spectrum 1 (b-1), the analyzed region corresponds to a bright-contrast, plate-like precipitate. The EDX results show high concentrations of Ni, Fe, and Cr, together with moderate-to-high levels of Nb and Mo, and a near-moderate amount of C. Based on both morphology and chemical composition, this precipitate is identified as a Laves phase. The elevated Ni, Fe, and Cr signals are most likely influenced by contributions from the surrounding γ matrix within the interaction volume, while the detected carbon is attributed to carbide precipitates present nearby.

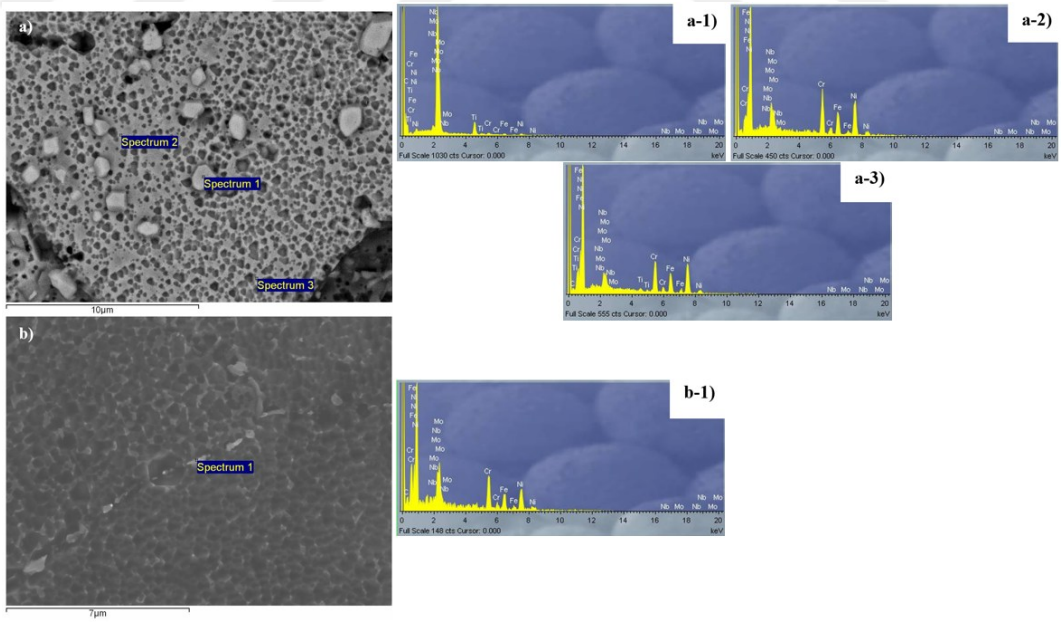

Figure 4.14. *SEM-EDX analysis results of etched heat-treated sample 6_S*

4.2.5. X-ray diffraction (XRD)

Phase composition analyses were carried out on two samples subjected to different heat treatment conditions, as shown in Figure 4.15 and Figure 4.16. The results revealed that the γ matrix was the dominant phase in all cases. In the as-HIPed condition, diffraction peaks obtained from both scrap and virgin Inconel 718 powders corresponded solely to the γ matrix. By contrast, in the heat-treated samples, additional phases such as γ″ and δ ($Ni_3(Nb,Ti)$) and Laves ($(Ni,Cr,Fe)_2(Nb,Mo,Ti)$) were identified. The SEM observations provide further confirmation of the presence of δ and Laves phases within the microstructure. These findings indicate that the applied heat treatment conditions require optimization, as the formation of such detrimental phases may negatively influence the alloy's performance.

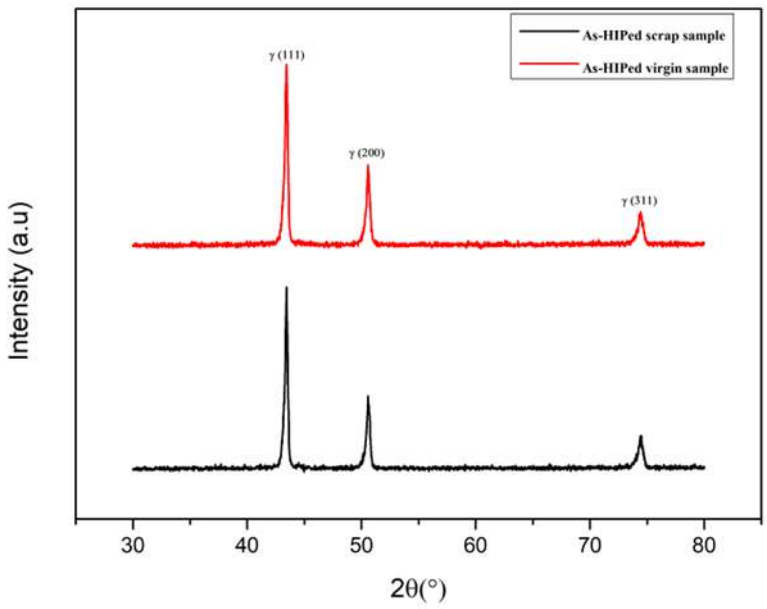

Figure 4.15. *XRD Analysis results of the as-HIPed samples*

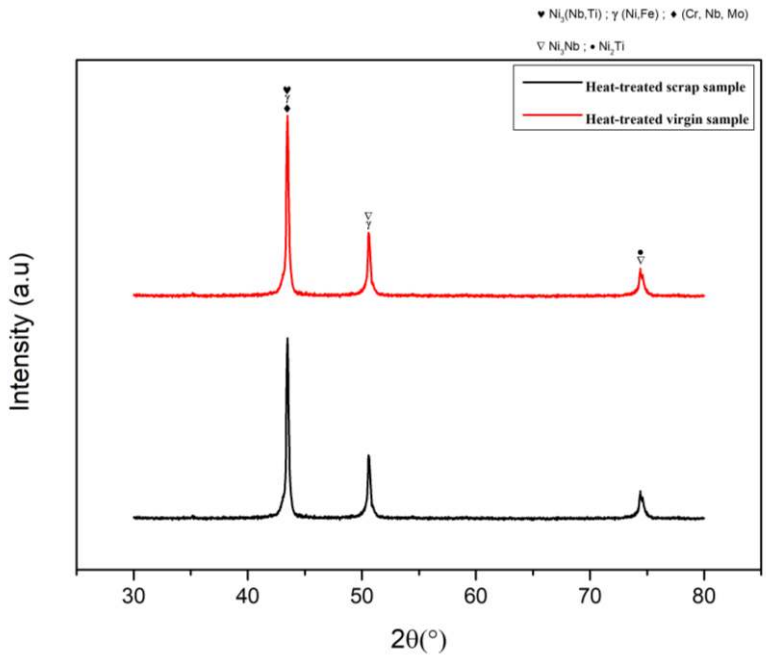

Figure 4.16. *XRD Analysis results of the heat-treated samples*

4.2.6. O/N elemental analysis

The results of the oxygen and nitrogen analyses performed to determine the O and N contents of the heat-treated samples are presented in Table 4.7. Examination of the data shows that the oxygen and nitrogen levels in these samples are significantly higher than those previously measured in the virgin and scrap Inconel 718 powders reported in Table 4.2. Given that the capsules were evacuated after filling and the HIP process was conducted within a sealed system, it is inferred that these increases in oxygen and nitrogen content primarily stem from the atmospheric heat treatments. The elevated temperatures used during these treatments in an open-atmosphere furnace facilitate the diffusion of oxygen and nitrogen from the surface into the bulk material.

Table 4.7. *Oxygen and nitrogen content determined by elemental analysis for the heat-treated samples*

Element	Virgin Inconel 718	Scrap Inconel 718
O (ppm)	236.23 ± 12.32	206.28 ± 7.13
N (ppm)	213.0 ± 19.80	1033.70 ± 91.25

4.2.7. Arc/spark optical emission spectrometry

The chemical compositions of the heat-treated samples were analyzed using arc/spark optical emission spectrometry (OES), with the results summarized in Table 4.8. Examination of the data indicates that the titanium content in samples fabricated from scrap Inconel 718 powders lies outside the specified range of 0.65–1.15 wt.% defined by ASTM F3055, as shown in the *Table **2.1***. These findings align with the XRF results previously reported for the virgin and scrap powders in Table 4.1.

A comparison between the results in Table 4.1 and Table 4.8 shows variations in the relative proportions of certain elements. However, these differences should not be interpreted as actual increases or decreases in elemental content. Instead, they stem from the measurement principle of arc/spark OES, which involves the vaporization and ionization of elements within the material. Variations in the vaporization and ionization behavior of specific elements can thus influence the reported concentrations.

Table 4.8. *Chemical composition of heat-treated samples determined by arc/spark optical emission spectrometry*

Element	Virgin Inconel 718	Scrap Inconel 718
C (wt.%)	0.0476 ± 0.004	0.0536 ± 0.0039
Si (wt.%)	0.1418 ± 0.003	0.1384 ± 0.0019
Mn (wt.%)	0.2504 ± 0.002	0.2806 ± 0.0036
P (wt.%)	0.0039 ± 0.0001	0.0037 ± 0.0001
S (wt.%)	< 0.001	< 0.001
Cr (wt.%)	18.912 ± 0.061	19.056 ± 0.0611
Fe (wt.%)	18.442 ± 0.079	18.994 ± 0.0647
Mo (wt.%)	3.114 ± 0.040	3.098 ± 0.0295
Cu (wt.%)	0.0099 ± 0.0002	0.0103 ± 0.0007
Co (wt.%)	0.0476 ± 0.0035	0.0383 ± 0.0009
Nb (wt.%)	5.178 ± 0.0646	5.186 ± 0.0555
Al (wt.%)	0.4644 ± 0.0021	0.4634 ± 0.0027
Ti (wt.%)	0.9142 ± 0.0080	0.6072 ± 0.0077
B (wt.%)	0.0012 ± 8.94	0.0013 ± 8.94
Ni (wt.%)	52.4 ± 0	51.7 ± 0.0707

4.2.8. Room temperature tensile test

Room temperature tensile tests were performed on the heat-treated samples to assess their mechanical behavior under tensile loading, with the results presented in Table

4.9. These values were compared against the minimum room temperature tensile property requirements outlined in SAE/AMS Standard 5663.

All samples produced from virgin Inconel 718 powders exhibited ultimate tensile strength (UTS) and yield strength (YS) values exceeding the SAE/AMS Standard 5663 minimum requirements of 1241 MPa and 1034 MPa, respectively. Furthermore, in agreement with the Archimedes density and optical porosity findings, a clear trend was observed wherein tensile strength decreased progressively from regions of higher to lower density.

In contrast, samples fabricated from scrap Inconel 718 powders, which showed significantly reduced densities, did not meet the minimum UTS requirement of 1241 MPa. Regarding yield strength, all samples satisfied the minimum criterion of 1034 MPa except for RT_7_S, RT_8_S, and RT_9_S.

It is noteworthy that none of the tested samples, regardless of powder type, achieved the SAE/AMS Standard 5663 specifications for elongation (≥ 10%) and reduction of area (≥ 12%). This is largely attributable to the fact that these standards are intended for forged materials, and variations inherent to the different production methods lead to certain mechanical properties meeting or exceeding the standard requirements while others fall short.

Table 4.9. *Mechanical properties obtained from room temperature tensile tests on the heat-treated samples*

Sample Name	Test Temperature (°C)	E (GPa)	U.T.S. (MPa)	0.2% Y.S. (MPa)	Elong.4D (%)	RA (%)
RT_1_V	25	185	1380	1160	6	5
RT_2_V	25	210	1380	1180	8	3
RT_3_V	25	187	1380	1190	6	7
RT_4_V	25	195	1370	1170	5	5
RT_5_V	25	190	1370	1170	5	4
RT_6_V	25	197	1370	1180	3	4
RT_7_V	25	202	1360	1160	6	5
RT_8_V	25	221	1340	1160	5	7
RT_9_V	25	210	1320	1200	6	3

Table 4.9. (Continued) *Mechanical properties obtained from room temperature tensile tests on the heat-treated samples*

Sample Name	Test Temperature (°C)	E (GPa)	U.T.S. (MPa)	0.2% Y.S. (MPa)	Elong.4D (%)	RA (%)
RT_1_S	25	185	1190	1070	3	2
RT_2_S	25	190	1200	1070	3	4
RT_3_S	25	183	1190	1070	5	1.6
RT_4_S	25	178	1160	1050	1.6	2
RT_5_S	25	187	1130	1050	1.6	0.6
RT_6_S	25	179	1060	1060	3	1.4
RT_7_S	25	182	1030	1010	3	0.6
RT_8_S	25	180	1020	995	1.6	0.6
RT_9_S	25	177	980	980	1.6	1.4

4.2.9. Elevated temperature tensile test

Elevated temperature tensile tests were performed on the heat-treated samples to assess their mechanical behavior under tensile loading and 649°C, with the results presented in Table 4.10. These values were compared against the minimum tensile property requirements at 649°C outlined in SAE/AMS Standard 5663.

All samples produced from virgin Inconel 718 powders exhibited ultimate tensile strength (UTS) and yield strength (YS) values exceeding the SAE/AMS Standard 5663 minimum requirements of 965 MPa and 862 MPa, respectively.

It is noteworthy that none of the tested samples, regardless of powder type, achieved the SAE/AMS Standard 5663 specifications for elongation (≥ 10%) and reduction of area (≥ 12%). This is largely attributable to the fact that these standards are intended for forged materials, and variations inherent to the different production methods lead to certain mechanical properties meeting or exceeding the standard requirements while others fall short.

In contrast, samples fabricated from scrap Inconel 718 powders, which showed significantly reduced densities, did not meet the minimum UTS requirement of 965 MPa. When looking at the yield strength results, it becomes clear that only sample ET_1_S meets the minimum threshold of 862 MPa. The other samples, however, fractured before any yielding could occur. This behavior is mainly attributed to their porous microstructure and insufficient bonding between particles. As a result, the samples couldn't undergo necking and broke apart without showing any signs of plastic deformation.

Table 4.10. *Mechanical properties obtained from elevated temperature tensile tests on the heat-treated samples*

Sample Name	Test Temperature (°C)	E (GPa)	U.T.S. (MPa)	0.2% Y.S. (MPa)	Elong.4D (%)	RA (%)
ET_1_V	649	180	1094	963	3.1	4.9
ET_2_V	649	207	1075	995	5	3.5
ET_3_V	649	193	1075	959	6.9	4.9
ET_4_V	649	189	1073	961	3.1	3.5
ET_5_V	649	196	1017	993	1.3	5.4
ET_1_S	649	164	892	870	1.3	3.9
ET_2_S	649	152	708	N/A	3.1	3.9
ET_3_S	649	165	693	N/A	3.1	5.4
ET_4_S	649	107	691	N/A	1.3	4.5
ET_5_S	649	123	631	N/A	3.1	3.9

4.2.10. High cycle fatigue test

The results of the high cycle fatigue (HCF) tests, performed to evaluate the fatigue life of the heat-treated samples under high-cycle, low-stress conditions, are summarized in Table 4.11. All tests were carried out at 650°C across three different stress levels.

The data show that samples HCF_1_V and HCF_2_V, extracted from high-density regions of samples fabricated with virgin Inconel 718 powder, exhibited infinite life at a stress level of 300 MPa. As expected, increasing the applied stress resulted in a corresponding decrease in fatigue life.

For samples produced from scrap Inconel 718 powder, sample HCF_1_S, taken from a relatively dense area, also demonstrated infinite life at 300 MPa. However, HCF_2_S, extracted from a similarly dense region, displayed significantly lower fatigue life under the same stress condition. This pronounced difference in performance for samples taken from closely situated regions suggests variability in local densification.

Moreover, as the applied stress increased, the fatigue life of samples made from scrap powders declined much more steeply compared to those produced from virgin powders, underscoring the critical influence of initial powder quality and uniformity on high-cycle fatigue behavior.

Table 4.11. *High cycle fatigue (HCF) performance of the heat-treated samples*

Sample Name	Test Temperature (°C)	Maximum Stress (MPa)	Life
HCF_1_V	650	300	1.00E+07
HCF_2_V	650	300	1.00E+07
HCF_3_V	650	450	1.88E+06
HCF_4_V	650	450	1.01E+06
HCF_5_V	650	650	6.93E+05
HCF_6_V	650	650	2.60E+05
HCF_1_S	650	300	1.00E+07
HCF_2_S	650	300	2869076
HCF_3_S	650	450	315077
HCF_4_S	650	450	255306
HCF_5_S	650	650	61567
HCF_6_S	650	650	1277

4.2.11. Stress-rupture test

As outlined in SAE/AMS Standard 5663, a sample is considered successful if it can endure a load of 690 MPa for a minimum of 23 hours without rupture.

In this study, none of the samples produced from either virgin or scrap Inconel 718 powders met that requirement, as shown in Table 4.12. This outcome is likely due to several factors: the manufacturing route used in this work differed from that specified in the standard, detrimental phases were present in the microstructure, and the scrap powder samples in particular exhibited lower overall density. Furthermore, a clear trend was observed, samples taken from lower density regions generally showed shorter.

Notably, the life of sample SR_3_S could not be measured, as it fractured at the threaded section where the test grips were applied right at the start of the test. This early failure is believed to be a result of the grip contacting an area of the sample with insufficient density.

Table 4.12. *Mechanical properties obtained from stress-rupture tests on the heat-treated samples*

Sample Name	Test Temperature (°C)	Maximum Stress (MPa)	Life (h)
SR_1_V	649	650	6.08
SR_2_V	649	600	10.59
SR_3_V	649	550	1.88

Table 4.12. (Continued) *Mechanical properties obtained from stress-rupture tests on the heat-treated samples*

Sample Name	Test Temperature (°C)	Maximum Stress (MPa)	Life (h)
SR_1_S	649	650	0.05
SR_2_S	649	600	0.15
SR_3_S	649	550	N/A

5. CONCLUSIONS

This study explored the potential for reusing Inconel 718 powders, deemed scrap due to repeated use or prolonged storage during additive manufacturing, through an alternative powder metallurgy route. The experimental work included powder characterization, capsule design and fabrication, filling the capsules with both virgin and scrap powders, consolidation via hot isostatic pressing (HIP), machining of samples, heat treatments, and detailed post-HIP analyses. Initial evaluations showed that while the virgin Inconel 718 powders met the compositional and physical requirements set by ASTM F3055, the scrap powders fell outside the acceptable limits. Following HIP and heat treatment (carried out in accordance with SAE/AMS Standard 5663), the consolidated samples were comprehensively examined to assess their mechanical, physical, chemical, and microstructural properties.

The results of the characterizations showed that physical changes in the powder material had a clear impact on sintering behavior, which in turn directly influenced the densification process. It became evident that powders exhibiting morphological imperfections require different sintering parameters than those with more ideal characteristics. In the as-HIPed billets, areas that were exposed earliest to temperature and pressure showed higher densification, while regions closer to the center of the capsule exhibited lower densification. These findings highlight the need for detailed parametric studies to identify optimal HIP conditions that ensure uniform densification throughout the material.

Following the HIP and subsequent heat treatment processes, the formation of detrimental phases, known to negatively impact mechanical performance, was clearly observed. It became apparent that mechanical behavior is governed not only by the material's density but also by the presence of these harmful phases. Moreover, the mechanical and physical properties of samples varied depending on their extraction location within the billets, indicating a degree of inhomogeneity in the final product. This lack of uniformity poses a significant limitation on the range of applications for which the material can be reliably used.

6. FUTURE STUDIES

Based on the overall findings of this study, several key steps are proposed to ensure that components manufactured from scrap Inconel 718 powder can deliver the necessary performance for their intended applications:

1) the development of near-net shape capsule geometries will be prioritized by implementing a robust and efficient encapsulation approach
2) the HIP process parameters will be fine-tuned to achieve billets with a relative density exceeding 99%, ensuring nearly complete densification
3) a thorough and application-specific material characterization protocol will be carried out to validate the suitability of the consolidated material for its designated use.

REFERENCES

[1] Akca, E., and Gürsel, A. (2015). A review on superalloys and IN718 nickel-based INCONEL superalloy. *Period. Eng. Nat. Sci*, *3*(1), 15-27.

[2] Raza, S. A., Canyurt, O. E., and Sezer, H. K. (2024). A systematic review of Inconel 939 alloy parts development via additive manufacturing process. *Heliyon*, *10*(3).

[3] Chang, L., Sun, W., Cui, Y., Zhang, F., and Yang, R. (2014). Effect of heat treatment on microstructure and mechanical properties of the hot-isostatic-pressed Inconel 718 powder compact. *Journal of alloys and compounds*, *590*, 227-232.

[4] Luo, S., Huang, W., Yang, H., Yang, J., Wang, Z., and Zeng, X. (2019). Microstructural evolution and corrosion behaviors of Inconel 718 alloy produced by selective laser melting following different heat treatments. *Additive manufacturing*, *30*, 100875.

[5] Bryndza, G., Tchuindjang, J. T., Chen, F., Habraken, A. M., Sepúlveda, H., Tuninetti, V., ... and Duchêne, L. (2025). Review of the Microstructural Impact on Creep Mechanisms and Performance for Laser Powder Bed Fusion Inconel 718. *Materials*, *18*(2), 276.

[6] Hosseini, E., and Popovich, V. A. (2019). A review of mechanical properties of additively manufactured Inconel 718. *Additive Manufacturing*, *30*, 100877.

[7] Le, W., Chen, Z., Yan, K., Naseem, S., Zhao, Y., Zhang, H., and Zhang, Z. (2021). Early evolution of δ phase and coarse γ phase in Inconel 718 alloy with high temperature ageing. *Materials Characterization*, *180*, 111403.

[8] Ferreri, N. C., Vogel, S. C., and Knezevic, M. (2020). Determining volume fractions of γ, γ′, γ ″, δ, and MC-carbide phases in Inconel 718 as a function of its processing history using an advanced neutron diffraction procedure. *Materials Science and Engineering: A*, *781*, 139228.

[9] Wlodek, S. T., and Field, R. D. THE EFFECTS OF LONG TIME EXPOSURE ON AL, L, OY 718.

[10] Zhao, Y., and Xiong, W. (2023). Influence of Homogenization on Phase Transformations during Isothermal Aging of Inconel 718 Superalloys Fabricated by Additive Manufacturing and Suction Casting. *Materials*, *16*(14), 4968.

[11] Ling, L. S. B., Yin, Z., Hu, Z., Liang, J. H., Wang, Z. Y., Wang, J., and Sun, B. D. (2019). Effects of the γ ″-Ni3Nb phase on mechanical properties of Inconel 718 Superalloys with different heat treatments. *Materials*, *13*(1), 151.

[12] Schirra, J. J., Caless, R. H., and Hatala, R. W. (1991). The Effect of Laves phase on the mechanical properties. *The Minerals, Metals and Materials Society*, 375-388.

[13] Aerospace, S. A. E. (2009). Aerospace material specification: AMS 5662. SAE International.

[14] Schneider, J., Lund, B., and Fullen, M. (2018). Effect of heat treatment variations on the mechanical properties of Inconel 718 selective laser melted samples. *Additive Manufacturing*, *21*, 248-254.

[15] Lambert, D. M. (2015, June). IN718 additive manufacturing properties and influences. In *JANNAF Propulsion Meeting* (No. M15-4526).

[16] Valencia, J. J. (1997). Sintering effect on the microstructure and mechanical properties of alloy 718 processed by powder injection molding. In *Proceeding of The 4th International Symposium on Superalloys 718, 625, 706 and Various Derivatives, Pittsburgh, 1997* (pp. 753-762). The Minerals, Metals and Materials Society.

[17] Zhang, J., Liu, J., Xu, D., Wu, J., Xu, L., and Yang, R. (2019). Characterization of the prior particle boundaries in a powder metallurgy Ti2AlNb alloy. *Journal of Materials Science and Technology*, *35*(11), 2513-2525.

[18] Chang, L., Sun, W., Cui, Y., and Yang, R. (2017). Preparation of hot-isostatic-pressed powder metallurgy superalloy Inconel 718 free of prior particle boundaries. *Materials Science and Engineering: A*, *682*, 341-344.

[19] Madejski, B., Malicki, M., Czarnewicz, S., and Gruber, K. (2020). Microstructural and mechanical properties of selective laser melted Inconel 718 for different sample sizes. *Fatigue of Aircraft Structures*, (12).

[20] Robertson, C., Lufkin, T. X., Pelton, R., Carter, A., and Wilkes, J. Next Generation Additive Manufacturing of Shrouded Turbine Wheel.

[21] Xu, J., Ma, T., Peng, R. L., and Hosseini, S. (2021). Effect of post-processes on the microstructure and mechanical properties of laser powder bed fused IN718 superalloy. *Additive Manufacturing*, *48*, 102416.

[22] Rao, G. A., Prasad, K. S., Kumar, M., Srinivas, M., and Sarma, D. S. (2003). Characterisation of hot isostatically pressed nickel base superalloy Inconel* 718. *Materials science and technology*, *19*(3), 313-321.

[23] Santecchia, E., Spigarelli, S., and Cabibbo, M. (2020). Material reuse in laser powder bed fusion: Side effects of the laser—Metal powder interaction. Metals, 10(3), 341.

[24] Moghimian, P., Poirié, T., Habibnejad-Korayem, M., Zavala, J. A., Kroeger, J., Marion, F., and Larouche, F. (2021). Metal powders in additive manufacturing: A review on reusability and recyclability of common titanium, nickel and aluminum alloys. Additive Manufacturing, 43, 102017.

[25] Saheb, S. H., Durgam, V. K., and Chandrashekhar, A. (2020, October). A review on metal powders in additive manufacturing. In AIP Conference Proceedings (Vol. 2281, No. 1). AIP Publishing.

[26] Sun, X., Chen, M., Liu, T., Zhang, K., Wei, H., Zhu, Z., and Liao, W. (2023). Characterization, preparation, and reuse of metallic powders for laser powder bed fusion: a review. *International Journal of Extreme Manufacturing*, *6*(1), 012003.

[27] Kaleem, M. A., Alam, M. Z., Khan, M., Jaffery, S. H. I., and Rashid, B. (2021). An experimental investigation on accuracy of Hausner Ratio and Carr Index of powders in additive manufacturing processes. *Metal Powder Report*, *76*, S50-S54.

[28] ASTM B212-21; Standard Test Method for Apparent Density of Free-Flowing Metal Powders Using the Hall Flowmeter Funnel. ASTM International: West Conshohocken, PA, USA, 2021.

[29] ASTM B527. (2006). Standard Test Method for Determination of Tap Density of Metallic Powders and Compounds. West Conshohocken, PA: American Society for Testing Materials.

[30] Vlachos, N., and Chang, I. T. (2011). Investigation of flow properties of metal powders from narrow particle size distribution to polydisperse mixtures through an improved Hall-flowmeter. *Powder technology*, *205*(1-3), 71-80.

[31] ASTM B213-20; Standard Test Methods for Flow Rate of Metal Powders Using the Hall Flowmeter Funnel. ASTM International: West Conshohocken, PA, USA, 2020.

[32] Ozeren, E., Bilgin, G. M., Ertekin, B., Taş, A., Cavcar, Z., Gökcan, M. B., ... and Kara, G. (2022). Characterization of metal powder reused multiple times for laser powder bed fusion. *Journal of Additive Manufacturing Technologies*, *2*(2), 688-688.

[33] Lanzutti, A., and Marin, E. (2024). The challenges and advances in recycling/re-using powder for metal 3D printing: A comprehensive review. *Metals*, *14*(8), 886.

[34] Thandalam, S. K., Ramanathan, S., and Sundarrajan, S. (2015). Synthesis, microstructural and mechanical properties of ex situ zircon particles (ZrSiO4) reinforced Metal Matrix Composites (MMCs): a review. *Journal of Materials Research and Technology*, *4*(3), 333-347.

[35] Liu, T., and Wang, Q. (2017). Functionally gradient intermetallic composites. *Intermetallic matrix composites properties and applications. Woodhea d Publishing*, 409-24.

[36] Angelo, P. C., Subramanian, R., and Ravisankar, B. (2022). *Powder metallurgy: science, technology and applications*. PHI Learning Pvt. Ltd..

[37] Li, S. S., Yue, X., Li, Q. Y., Peng, H. L., Dong, B. X., Liu, T. S., ... and Jiang, Q. C. (2023). Development and applications of aluminum alloys for aerospace industry. *Journal of materials research and technology*, *27*, 944-983.

[38] Zimmerman, F. X., and Toops, J. (2008). Hot isostatic pressing: today and tomorrow. *Avure Technologies, www. avure. com*.

[39] ElRakayby, H., and Kim, K. (2018). Effect of glass container encapsulation on deformation and densification behavior of metal powders during hot isostatic pressing. *International journal of material forming*, *11*, 517-525.

[40] Atkinson, H. V., and Davies, S. (2000). Fundamental aspects of hot isostatic pressing: an overview. *Metallurgical and materials transactions A*, *31*, 2981-3000.

[41] Downing, M. (1993). A new powder encapsulation method and its implications on densification by hot isostatic pressing.

[42] Sobhani, S., Albert, M., Gandy, D., Tabei, A., and Fan, Z. (2023). Design optimization of hot isostatic pressing capsules. *Journal of Manufacturing and Materials Processing*, *7*(1), 30.

[43] Hoelzer, D. T. The Use of Powder Metallurgy and Hot Isostatic Pressing for Fabricating Components of Nuclear Power Plants,(2022). *ORNL/SPR-2022/2421*.

[44] Chung, S. H., Park, H., Jeon, K. D., Kim, K. T., and Hwang, S. M. (2001). An optimal container design for metal powder under hot isostatic pressing. *J. Eng. Mater. Technol.*, *123*(2), 234-239.

[45] Fitzpatrick, J. (2024). Powder properties in food production systems. In *Handbook of food powders* (pp. 203-218). Woodhead Publishing.

[46] Rao, G. A., Srinivas, M., and Sarma, D. S. (2006). Effect of oxygen content of powder on microstructure and mechanical properties of hot isostatically pressed superalloy Inconel 718. *Materials Science and Engineering: A*, *435*, 84-99.

[47] Pauzon, C., Markström, A., Dubiez-Le Goff, S., and Hryha, E. (2021). Effect of the process atmosphere composition on alloy 718 produced by laser powder bed fusion. Metals, 11(8), 1254.

[48] RECYCLING, P. (2019). ELECTRON BEAM MELTING OF ALLOY 718.

[49] Bu, H., Chen, L., and Duan, Y. (2022). Effect of solution heat treatment on the porosity growth of nickel-based P/M superalloys. Metals, 12(11), 1973.

CURRICULUM VITAE

ORCID : 0009-0007-4530-666X

Name/Surname : Yağmur Can Gündoğan

EDUCATION

Master's degree (Sep 2022 – Continues)
Eskişehir Technical University
Materials Science and Engineering Programme

Bachelor's degree (Sep 2017 – Jan 2022)
Eskişehir Technical University
Department of Materials Science and Engineering

PROFESSIONAL EXPERIENCE

Composite Development Engineer (Sep 2022 – Continues)
TUSAŞ Engine Industries, Inc.
R&D and Innovation Department